
Article:
Isteri, V., Ohenoja, K., Hanein, T. orcid.org/0000-0002-3009-703X et al. (4 more authors) (2020) Production and properties of ferrite-rich CSAB cement from metallurgical industry residues. Science of The Total Environment, 712. 136208. ISSN 0048-9697

https://doi.org/10.1016/j.scitotenv.2019.136208

Journal Pre-proof

Production and properties of ferrite-rich CSAB cement from metallurgical industry residues

Visa Isteri, Katja Ohenoja, Theodore Hanein, Hajime Kinoshita, Pekka Tanskanen, Mirja Illikainen, Timo Fabritius

PII: S0048-9697(19)36204-7

DOI: https://doi.org/10.1016/j.scitotenv.2019.136208

Reference: STOTEN 136208

To appear in: *Science of the Total Environment*

Received date: 15 October 2019

Revised date: 16 December 2019

Accepted date: 17 December 2019

Please cite this article as: V. Isteri, K. Ohenoja, T. Hanein, et al., Production and properties of ferrite-rich CSAB cement from metallurgical industry residues, *Science of the Total Environment* (2019), https://doi.org/10.1016/j.scitotenv.2019.136208

Production and properties of ferrite-rich CSAB cement from metallurgical industry residues

*Visa Isteri[a], Katja Ohenoja[*b], Theodore Hanein[c], Hajime Kinoshita[c], Pekka Tanskanen[a], Mirja Illikainen[b], and Timo Fabritius[a*]*

[a] Process metallurgy, Faculty of Technology, PO Box 4300, 90014 University of Oulu, Finland

[b] Fibre and Particle Engineering, Faculty of Technology, PO Box 4300, 90014 University of Oulu, Finland

[c] Department of Materials Science and Engineering, The University of Sheffield, Sheffield S1 3JD, UK

**corresponding author: Timo Fabritius (timo.fabritius@oulu.fi)*

Keywords: CSA cement; fayalite slag; fluorellestadite; jarosite; steel making slag; utilization

Highlights

- CSAB clinkers were produced using metallurgical residues
- Fe and fayalitic slag are used to make CSAB with ye'elimite, belite, and ferrite
- The fluorine content in AOD slag enabled the formation of fluorellestadite
- Compressive strength of the produced CSAB mortars is comparable to commercial PC

Abstract

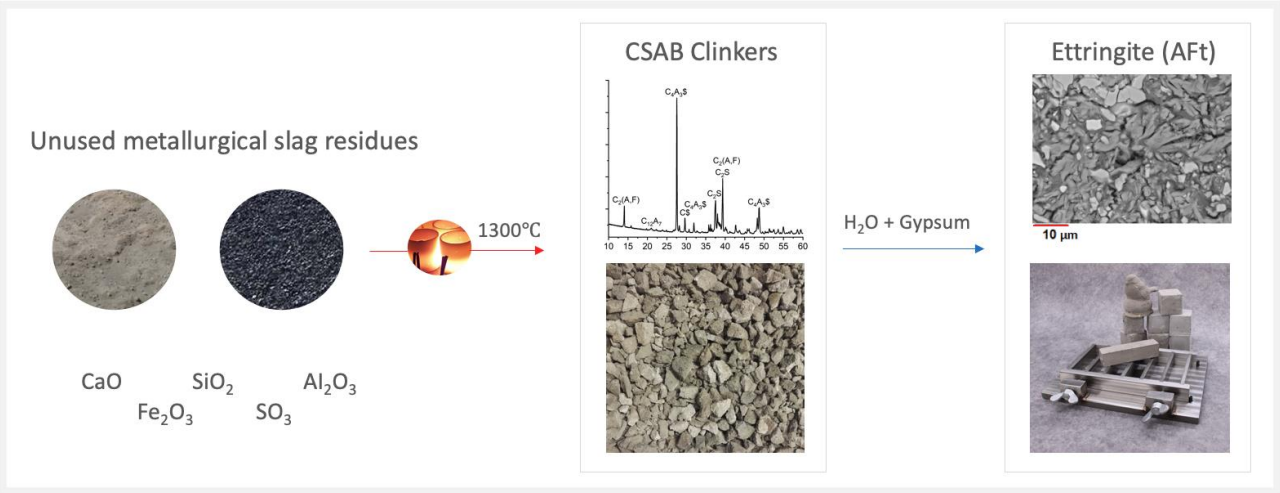

Blast furnace slag from the steel industry is commercially utilized as a cement replacement material without major processing requirements; however, there are many unutilized steel production slags which differ considerably from the blast furnace slag in chemical and physical properties. In this study, calcium sulfoaluminate belite (CSAB) cement clinkers were produced using generally unutilized metallurgical industry residues: AOD (Argon Oxygen Decarburisation) slag from stainless steel production, Fe slag from zinc production, and fayalitic slag from nickel production. CSAB clinker with a target composition of ye'elimite-belite-ferrite was produced by firing raw materials at 1300 °C. The phase composition of the produced clinkers was identified using quantitative XRD analyses, and the chemical composition of the clinker phases produced was established using FESEM-EDS and mechanical properties were tested through compressive strength test. It is demonstrated that these metallurgical residues can be used successfully as alternative raw materials for the production of CSAB cement that can be used for special applications. In addition, it is shown that the available quantities of these side-streams are enough for significant replacement of virgin raw materials used in cement production.

Abbreviations

AAS - Aluminium anodizing sludge

AOD - Argon Oxygen Decarburisation

AOD_C - CSAB clinker produced from reagent grade chemicals and AOD slag

CO_2e - Equivalent CO_2 emissions

BCSA - Belite calcium sulfoaluminate

BOF - Basic oxygen furnace

BSE - Back-scattered electron detector

CSA - Calcium sulfoaluminate

CSAB - Calcium sulfoaluminate belite

Fay_C - CSAB clinker produced from reagent grade chemicals and fayalitic slag

Fe_C - CSAB clinker produced from reagent grade chemicals and pyrometallurgically treated jarosite

EAFS - Electric arc furnace slag

EDS - Energy-dispersive X-ray spectroscopy

ICDD - The International Centre for Diffraction Data

ICP-OES - Inductively coupled plasma atomic emission spectroscopy

FESEM - Field emission scanning electron microscope/microscopy

FGD - Flue gas desulfurization

PC - Portland cement

PDF - Powder Diffraction File

LOI – Loss on ignition

RGC - Reagent grade chemicals

RC_C – CSAB clinker produced from reagent grade chemicals

SCM's - Supplementary cementitious materials

TGA - Thermal gravimetric analysis

UNEP - SBCI -United Nations environment programme (UNEP) - Sustainable Buildings & Climate Initiative

WPPF - Whole Powder Pattern Fit

XRD - X-ray Diffraction

XRF - X-ray fluorescence

Introduction

Population growth and urbanization increases the demand to expand our built environment (Miller et al., 2016) in which concrete is the fundamental building material (WBCSD, 2009). Cement is the key binding component in concrete, and global cement production was estimated to be 4.1 billion tons in 2017 (Cembureau, 2018). The most commonly used binder is Portland cement (PC), in which the major and characteristic mineral phase is alite (C_3S)[1] (Taylor, 1997). PC manufacture emits approximately 0.87 tons equivalent carbon dioxide (CO_2e) per ton of cement (Hanein et al., 2018). CO_2 emissions arise primarily from the calcination of limestone, which is mainly $CaCO_3$, during the firing process, and secondarily from the burning of fossil fuels necessary to achieve the required firing temperature, which is approx. 1450 °C in conventional PC production (Gartner and Hirao, 2015).

The growing demand for cement, coupled with increasing environmental awareness, has led to increased focus from the cement community on mitigation strategies. The UNEP SBCI-report concludes that the most promising ways to decrease CO_2 emissions related to cement production are 1) increased use of supplementary cementitious materials (SCM's) and 2) more efficient use of PC. Alternative non-Portland clinkers were also proposed to provide substantial reduction of CO_2 emissions (Scrivener et al., 2018).

[1] The cement oxide chemistry notation used in this work: C = CaO, S = SiO_2, A = Al_2O_3, F = Fe_2O_3, and $ = SO_3.

One of the alternative, lower-carbon clinkers is calcium sulfoaluminate (CSA) cement that is based on less calcium-containing cementitious phases such as ye'elimite ($C_4A_3\$$), belite (C_2S), and ferrite ($C_2(A,F)$) (Álvarez-Pinazo et al., 2013; Gartner and Hirao, 2015; Miller et al., 2018). The variations of CSA cements can be classified according to the main crystalline phases of the clinkers that they consist of (Álvarez-Pinazo, 2015). In this study, CSAB (calcium sulfoaluminate-belite) refers to the cements with ye'elimite ($C_4A_3\$$) as the main phase and belite (C_2S) as the secondary phase; compositions also contain ferrite ($C_2(A,F)$) and anhydrite ($C\$$).

CSA cements have been manufactured commercially in China since the 1970s under the name "third cement series" (Zhang et al., 1999). In the United States of America, belite calcium sulfoaluminate (BCSA) cement has been successfully used for pavement rehabilitation of interstate highways for the past 40 years (Bescher et al., 2018). Recently the interest to use these low CO_2 cements has been growing. As shown in the work by Hanein et al., 2018, the benefit of CSA cements is that they have less $CaCO_3$-related CO_2 emissions through reduced usage of limestone and lower production energy required. Hanein et al., 2018 concluded that the overall, net emissions can be reduced 25–35% when CSA cements are produced as alternative to PC. The main drawback of these CSA cements is the requirement of aluminium-rich raw materials, which are typically more expensive, and their availability have locational limitations. The assemblage of clinker composed from ye'elimite, belite, and ferrite phases allows for the employment of industrial side-streams in their manufacture, which would otherwise go into landfills (Chen, 2009).

The use of industrial side-streams in CSA clinker production can decrease the costs and increase local availability of the raw materials. However, the side-streams must be available locally to avoid transportation costs. Different industrial processing plants use different raw materials and manufacturing methods for their products; thus, producing varied side-streams. When these industrial side-streams are to be used as raw materials for CSAB cement production, the usability of a specific raw material and clinkering parameters should be tested and proven for the unique impurities and mineralogy of the side-stream materials which can affect cement clinker production and the properties of the hydrated product.

Several studies examine the use of alternative raw materials such as industrial side-streams or side-streams to manufacture CSA cement. Hanein et al. (2016) utilized sulfur, a side-stream of the Claus process, both as a fuel and source of clinker SO_3 to produce CSAB cements. Other studies focused on substituting $CaCO_3$ and relatively expensive bauxite respectively with CaO-bearing materials. This was done to reduce CO_2 emissions and Al_2O_3-containing materials to lower raw material costs. El-Alfi and Gado (2016) used marble sludge with high CaO content to prepare CSAB cement at 1250 °C. Chen and Juenger (2012) successfully synthesized side-stream material based CSAB cement using flue gas desulfurization (FGD) sludge, class C fly ash, and fluidized bed ash; however, they noted that impurities in raw materials could significantly affect CSAB cement formation, hydration, and properties. Da Costa et al. (2016) used aluminium anodizing sludge (AAS) to replace bauxite and achieved good mechanical properties with their clinkers; however, they underlined that the use of alternative aluminium sources can affect the clinkerisation process through the incorporation of foreign ions such as Na, K, and Mg. Iacobescu et al. (2013) produced high ferrite containing CSAB cement using electric arc furnace slag (EAFS) at 1320 °C; they found that their cements had good mechanical properties when they used 10-17 wt% EAFS (C_4AF 33.0-38.9 wt%) together with FGD gypsum; but, a higher amount of EAFS led to poor mechanical properties. Adolfsson et al., (2007a, 2007b) produced CSAB cement by making four different mixtures from basic oxygen furnace (BOF) converter slag, EAFS, argon oxygen decarburisation (AOD) slag, ladle slag, gypsum, alumina, and limestone; they showed that there is potential in using metallurgical slags as a raw material for CSAB cement manufacture. When 14% of AOD slag was used to raw material mixture the major phases of CSAB could be synthesized but with 55% of AOD slag the major phases were ye'elimite and bredigite ($Ca_7Mg(SiO_4)_4$); the latter having slow hydration and thus undesirable.

The use of AOD slag as raw material for CSAB cement production showed that the major phases of CSA could be synthesized from the material (Adolfsson et al., 2007a); however, their study did not contain information on the effect of foreign elements e.g. fluorine on the clinkering properties of CSAB cement. The literature is lacking in studies of using Fayalitic slags and Fe slags as raw materials for CSAB cement manufacture; although, some studies assessed the use of fayalitic slags as SCM's to replace PC (Rahman et

al. 2017) and as raw materials for geopolymers (Maragkos et al. 2009). In this work, these three varied metallurgical residues are tested separately with reagent grade chemicals (RGC) to understand how they affect CSAB clinker properties individually. The aim of this study is to assess how the properties of clinkers changes when certain impurities are added to the system through using these industrial side-stream materials.

The CSAB clinkers manufactured in this study are intended for special applications e.g. mine backfilling, waste handling and industrial infrastructure. The hydration product of CSAB cement, ettringite, is known to encapsulate/stabilize heavy metals and other hazardous components (Chrysochoou and Dermatas 2006; Kumarathasan et al., 1989; Peysson et al. 2005) and can enable the control of hazardous components in raw materials and also to stabilize hazardous components in other added materials such as mine tailings (Kiventerä et al. 2019). The target phase composition of the CSAB clinker is 40% ($C_4A_3\$$), 35% (C_2S), 20% (C_2F), and 5% C$. Three different slags along with reagent grade chemicals are used to prepare 1.5 kg of four different clinkers. The clinkers are then characterized via XRF, XRD (coupled with Rietveld calculations), and FESEM-EDS. The mechanical properties of cement mortars were tested via compressive strength tests and selected cured cement pastes were analysed through FESEM-EDS analysis.

Materials and methods

2.1 Materials

Four CSAB cement clinkers with the same target phase composition were manufactured from reagent-grade chemicals and Finnish metallurgical industrial side-streams. Details of the reagent grade chemicals used are provided in Table 1.

Table 1. Details of reagent grade chemicals used for clinker synthesis.

		Purity (wt%)	CAS-number
Aluminium oxide (metals basis), fine powder	Al_2O_3	99	12553

Silicon (IV) Oxide (metals basis), Mesh fused amorphous powder	SiO_2	99	89709
Iron (III) oxide (metals basis)	Fe_2O_3	98	012375
Calcium sulphate, anhydrous powder	$CaSO_4$	99	40144
Calcium oxide, reagent-grade powder	CaO	98	33299

The Finish industrial side-streams used were: Argon Oxygen Decarburisation (AOD) slag resulting from the steel refining process at Outokumpu Stainless Oy (Tornio), fayalitic slag from the nickel flash furnace process at Boliden Harjavalta, and Fe slag from the pyrometallurgically treated jarosite at Kokkola Boliden. AOD is the generally employed process to refine stainless steel melt. The mineralogical composition of general AOD slag consist of C_2S, C_3S, calcium-aluminium silicates, $CaCO_3$, free lime, periclase, and cuspidine ($Ca_4(Si_2O_7)(F,OH)_2$) (Adegoloye et al., 2015; Durinck et al., 2008; Shen et al., 2004). The metallic oxide components (Fe, Cr, and Ni) in AOD slag are present as magnetite and chromite, or chromium spinel. AOD slag also contains metal droplets in forms of Fe-Ni alloy, Fe-Cr-Ni alloy, and stainless steel (Adegoloye et al., 2015; Durinck et al., 2008; Shen et al., 2004). Even after successful reduction, the slag still contains small amounts of Cr_2O_3, which limits its application because of the risk of leaching (Di Maria et al., 2018; Huaiwei and Xin, 2011; Shen et al., 2004; Zhao et al., 2013). Another problem in direct utilization of AOD slag is dusting of C_2S during cooling of the slag (Seki et al., 1986). For this study, metal particles were removed from AOD slag and slag was ground by a contractor of the steel plant without describing. The fayalitic slag originates from a flash-smelting furnace process where nickel concentrate is smelted to produce nickel matte. After flash smelting, the slag is cleaned within a reductive electric furnace to recover Ni and Co from the slag, and the slag is granulated with water to d=80 mm particles. The mineralogical composition of Fayalitic slag consists of >60% of amorphous glass; the rest is crystalline fayalite and a few percent of magnetite. The Fe slag used for this study is a modified jarosite from zinc production. The chemical formula of jarosite is $MFe_3(SO_4)_2(OH)_6$ where M is Ag^+, $H3O^+$, K^+, Li^+, Na^+, NH^{4+},or $1/2Pb^{2+}$ (Dutrizac, 1984). For this study, the pyrometallurgically treated jarosite residue (Fe slag) is synthesized with the method introduced in the study of Rämä et al. (2018). The jarosite was treated with laboratory-scale pyrometallurgical

oxidation-reduction at 1400 °C. The aim of the pyrometallurgical treatment is to recover valuable metals from jarosite residue and to obtain clean inert slag, which could be used for construction purposes (Rämä et al., 2018). The mineralogical composition of Fe slag consists of Ca-Fe silicate and magnetite. The main chemical components and impurities of the side-stream materials are shown in Table 2. The main phases of Fayalitic and Fe slags have olivine structure where iron is present as FeO, during clinkering FeO is assumed to oxidize to Fe_2O_3. Before grinding, AOD slag was sieved through 500 µm sieve; metal droplets were not detected. AOD slag and fayalite slag were ground with stainless steel jar mill (10 L) for 1 hour using 120 stainless steel balls (d=30 mm) to make sure that the particle size of the slags are homogenous, estimation for particle size D_{50} <10 µm. Fe slag was crushed/ground using vibratory disc mill, the estimation for particle size D_{50} <200 µm.

Table 2. Analysis of side-stream raw materials.

XRF oxide composition wt%			
Compounds for CSAB	AOD slag	Fayalitic slag	Fe slag
CaO	53.2	1.8	16.8
SiO_2	28.0	33.5	29.9
FeO	0.6	52.9	35.5
Al_2O_3	1.7	2.3	5.0
SO_3	0.4	0.2	0.8
Other compounds			
MgO	8.72	6.23	3.01
TiO_2	0.34	0.15	0.49
CaF_2	3.2	0.0	0.0
Na_2O	0.0	0.39	2.75
Others (wt. % < 0.8)	1.19	2.3	3.7

ICP analysis results wt%			
Ba	0.02	<0.01	0.53
Mn	0.14	0.02	0.46
Cr	0.08	0.04	0.05
Cu	<0.01	0.06	0.25
Ni	<0.01	<0.4	0.05
Co	<0.01	<0.4	0.02
Zn	<0.01	0.02	0.51

2.2 Methods

2.2.1 Analysis of materials

Prior to preparation of melt-fused beads, loss on ignition (LOI) was measured using thermogravimetric analysis (TGA) using Prepash Precisa Gravimetrics AG: "prepASH automatic drying and ashing system". The heating cycle in TGA was 30 min ramp to 105 °C/4 h hold, 2 h 30 min ramp to 525 °C/3 h hold and 1 h ramp to 950 °C/3 h hold. For melt-fused beads, 1.5 g of each LOI treated side-stream material and clinker were mixed separately in a platinum crucible with 7.5 g of X-ray flux Type 66:34 (66% LiB_4O_7 and 34% $LiBO_2$). The melt fused beads were prepared using a Pananalytics Eagon 2 fluxer. The following sequences were used during fluxing: melting 1150 °C/120 s, mixing for 480 s with rocking angle 45°, injecting of the releasing agent for 240 s, pouring duration was 15 s with angle 135°, and the fan cooling for 120 s. Before XRF analysis, the samples were ground with a planetary mill with 300 rpm for 1 min. The X-ray fluorescence (XRF) from a melt-fused bead was operated using an Omnian Pananalytics Axiosmax 4 kV to determine the main chemical components of side-stream materials and clinkers.

Before XRD analysis, each clinker was ground to a fine powder by hand using an agate mortar for 20 min and then loaded into powder sample holders. The XRD patterns were collected using a Rigaku SmartLab 9 kW diffractometer in the Bragg-Brentano geometry. The diffractometer was operated at 40 kV and 135 mA and is equipped with Co K_α X-ray source ($K_{\alpha1}$=1.78892, $K_{\alpha2}$=1.79278) and D/teX Ultra 250 detector Co Kα

radiation source was used because of iron content in the samples. Kβ radiation was reduced with a filter. The XRD-patterns were measured from 5.0° to 120.0° 2-theta with a step size of 0.02° and scanning speed 5°/min; the total scan time was 24 min. A quantitative analysis to identify crystalline phases was performed using Rigaku PDXL 2 software that compares the diffraction patterns on the ICDD (PDF-4+ 2019 RDB) database using WPPF (Whole Powder Pattern Fit) analysis with Rietveld method; the lattice parameters and profile were refined, all peaks are manually checked and the crystallographic information files are selected based on literature, elemental composition, and knowledge from supporting analyses (FESEM and XRF). The WPPF analysis finds the best agreement between measured and calculated diffraction pattern through simultaneous refinement of models for diffraction optics, instrumental parameters, background, phase specific parameters (cell parameters and crystal structure) and sample specific parameters (crystallite size, stress and preferred orientation). The model functions during the analysis were as follows: background = b-spline; peak-shift = shift axial displacement; peak shape function= split pseudo-Voigt and preferred orientation = March-Dollase. The WPPF analysis gives the phase composition normalized to 100% and the quality of analysis is determined from the weighted pattern R-factors (Rwp) and goodness of fit indicator (S-value). The sources to crystallographic files for cement phases are presented with the Rietveld results.

Polished sections for field emission scanning electron microscope (FESEM) analysis were prepared by using optical-grade epoxy resin (Struers Epofix). First, a piece of cement clinker was submerged in epoxy resin in a cylindrical 40 mm mould under vacuum and the cast was placed in a 40 °C oven for 24 h to allow the epoxy to cure. After curing, a thin section was cut from the middle of the 40 mm cast. The cut thin section was placed to a 25 mm cylindrical mould, impregnated with epoxy resin in a vacuum and cured with same parameters. After curing, extra epoxy from the top of the cast was cut down, using a lathe and the bottom of the sample was polished with a wheel polisher (Struers LaboPol-6). Instead of water, 98% pure ethanol was used as lubricant/coolant. The polished sections were coated with carbon to achieve electrical conductivity. A FESEM (Zeiss Ultra Plus) equipped with an energy-dispersive X-ray spectroscopy (EDS) analysis system and back-scattered electron detector (BSE) was used to analyse phase distribution in CSAB clinkers. Configuration was operated with acceleration voltage of 15 kV, current 3.2-4.8 nA, and working

distance between 7.3-8.0 mm. AZtec software (Oxford Instrument) was used to analyse the BSE pictures and the elemental chemical composition of the selected EDS points. The amount of each chemical element was received as weight percent.

Trace elements of industrial side-stream materials were measured with inductively coupled plasma atomic emission spectroscopy (ICP-OES). The microwave-assisted wet digestion was performed using a 3:1 ratio of HNO_3 and HCl acid mixture for 0.5 g of AOD slag, Fe Slag, and fayalitic slag at 175 °C according to EPA3051A (United States Environmental Protection Agency, 2007).

For compressive strength tests, cements mortars were prepared according to cement standard (EN 196-1, 2005). Due to limited amount of material availability, 2 x 2 x 8 cm prisms were used instead of 4 x 4 x 16 cm prisms. Cement mixtures for mortars were mixed by using 85% clinker (AOD_C, Fay_C, Fe_C, RG_C) and 15% gypsum. Mortars were prepared using lab scale cement mixer (65-L0006/AM AUTOMIX) using prepared cement mixes, standard sand and tap water with cement to water ratio of 0.5. Mortars were cured in 98% air humidity at room temperature for 1, 7 and 28 days prior to being tested. Three parallel 2 × 2 × 8 cm mortar prisms were cut to two halves using precision cutting machine (Struers Secotom 10). Each half was then used for the unconfined compressive strength tests, totalling six measurements for each type of mortar. Tests were operated using Zwick testing machine with a maximum load of 100 kN, here employing a loading force of 2.4 kN/s. The reference samples from commercial PC (CEM II/A-LL 52.5 N) was mixed according to standard EN 196-1 and also tested with 2 x 2 x 8 cm prisms after 7 and 28 days of curing.

2.2.2 Clinker preparation

Stoichiometric calculations were used to estimate the amount of raw material oxides used to prepare the CSAB cement clinker. The following assumptions were carried out for the calculations:

- C_2F is the only phase that contains iron (Fe_2O_3=C_2F (wt%) /(C_2F (g/mol)/Fe_2O_3 (g/mol))
- C_2S is the only phase that contains SiO_2 (SiO_2=C_2S (wt%) /(C_2S (g/mol)/SiO_2 (g/mol))

- $C_4A_3\$$ is the only phase that contains alumina (Al_2O_3=$C_4A_3\$$ (wt%)/($C_4A_3\$$ (g/mol)/3*Al_2O_3 (g/mol))
- SO_3 in excess remains as C$ (SO_3=$C_4A_3\$$ (wt%)/($C_4A_3\$$ (mol)g//SO_3(g/mol))+C$ (wt%)/(C$(g/mol)/$SO_3$(g/mol))
- CaO required is the sum of CaO in empirical formula of single phases multiplied with the target amount of each phase

The target composition is presented in Table 3. Based on prior knowledge, excess free lime should be added to prevent gehlenite formation and extra SO_3 to compensate possible SO_3 loss during firing and to maximize ye'elimite formation over mayenite. In cement chemistry, ferrite generally refers to tetracalcium aluminoferrite (C_4AF), which represents one point of the actual solid solution series (Redhammer et al., 2004). The common mineral name for Ferrite is brownmillerite $Ca_2Al_xFe_{2-x}O_5$. Ferrite appears with various Al/Fe ratios and ionic substitutions (Taylor, 1997). At atmospheric pressure, a ternary continuous solid-solution series $Ca_2Al_xFe_{2-x}O_5$ can exist in the compositional range $0.0 \leq x \leq 1.4$ (Geller et al., 1971; Redhammer et al., 2004; Smith, 1962; Taylor, 1997). Due to iron content of the residues (Table 2), x=0 was selected to maximize the iron content in the solid-solution series and allow the Al to be fully exploited in a more cementitious phase, ye'elimite. Our target ferrite phase in this study is $Ca_2Fe_2O_5$ (C_2F).

Table 3. Phase composition of target CSAB clinker and corresponding oxide composition.

Target phase composition					
Phase	C_2F	$C_4A_3\$$	C_2S	C$	C
[wt%]	17	41	35	6	1
Corresponding oxide composition					
Oxide	Fe_2O_3	Al_2O_3	SiO_2	SO_3	CaO
[wt%]	10	20	12	9	49

Four different CSAB clinkers were prepared. Three clinkers were produced using industrial side-streams (AOD_C, Fay_C, and Fe_C) and one control sample was produced from reagent grade chemicals (RGC)

alone. Each starting mixture was prepared based on the corresponding industrial slag mixed with the reagent grade chemicals necessary to achieve the target clinker composition; see Table 4.

Table 4. Clinker recipes, the values are given in %.

Sample	RG_C	AOD_C	Fay_C	Fe_C
AOD slag		43.3		
Fayalitic slag			17	
Fe slag				25.3
Al_2O_3	20.3	19.5	19.9	19
SiO_2	12.2		6.5	4.6
$CaSO_4$	15.3	15	15.2	15
CaO	42.3	18.4	42	38.2
Fe_2O_3	10	9.7		
SUM + Impurities [%]	100	105.9	100.6	102.1

In Table 4, the amount of raw material in industrial side-stream clinkers is over 100 % because the impurities of raw materials were not taken account in the calculation of main oxides of target compositions. The amounts of main impurities in 100 % of clinkers (Table 5) were calculated from XRF and ICP analysis results of raw materials (Table 2). MgO was the main "impurity" in all raw materials. In AOD slag, MgO came from a slag-forming agent (dolomitic lime) that is added to process and from the wearing of refractory materials. In fayalitic and Fe slag, MgO originates from the raw material feed. In addition, all the raw materials include minor quantities of various impurities as shown in Table 5.

Table 5. The impurities from raw materials to clinkers, the values are given in %.

XRF	AOD_C	Fay_C	Fe_C

MgO	3.77	1.05	0.78
K_2O	0.13	0.09	0.10
TiO_2	0.13	0.03	0.13
CaF_2	1.37	n.d.	n.d.
Na_2O	n.d.	0.07	0.71

ICP	AOD_C	Fay_C	Fe_C
Ba	<0.01	<0.01	0.13
Mn	0.06	<0.01	0.12
Cr	0.03	<0.01	0.01
Cu	<0.01	<0.01	0.06
Ni	<0.01	0.02	0.01
Co	<0.01	0.01	<0.01

Before weighing the components, CaO was calcined at 800 °C for four hours to remove possible moisture and/or CO_2 that may have interacted with it. Calcium sulphate was dried at 250 °C for two hours, and all the side-stream raw materials were ground with a ball mill and dried at 105 °C for 24 h. Raw materials were weighed to produce 1.5 kg of each clinker. The materials for each clinker were mixed in a stainless-steel bowl and sieved several times. After mixing, raw material mixtures of each type of clinker were compressed in three cylinder-shaped corundum crucibles by hand.

Clinkering (firing) was conducted in a Nabertherm chamber furnace. The crucibles were placed within a furnace pre-heated to 800 °C, then heated 10 °C/min to 1300 °C, and then held for 4 hours. After, the crucibles were taken out. To achieve faster cooling, the crucibles were placed on a copper table with water circulation.

3. Results and discussion

3.1 Clinker visual characterization

After firing, it was observed that AOD_C clinker differed from the other clinkers produced. The indurated AOD_C clinker "cake" was remarkably hard to grind, where other clinkers were friable and easy to grind.

The visually observed melting or more advanced sintering behaviour in AOD_C (Fig. 1) can be explained with presence of fluorine, which is known to work as flux or mineralizer in Portland cement and modified Portland cements (Blanco-Varela et al., 1995; Odler and Zhang, 1996; Shame and Glasser, 1987). Flux lowers the initial liquid formation temperature and mineralizer can lower the formation temperature of minerals. (Blanco-Varela et al., 1995; Duvallet, 2014a).

Fig. 1. Left; AOD_C after firing and removing from the crucible. Right; Fe_C after firing and crushing with hammer.

3.2 XRD analysis

After visual analysis, clinkers were ground using a tumbling ball mill and the phase contents of each produced clinker were determined using XRD and quantified with the Rietveld method. The XRD-patterns with the six main phases are shown in Fig. 2, and the results of Rietveld analysis with major and minor phases are presented in Table 6. The presented diffraction patterns are limited to 10-55° in order to make the data discernible.

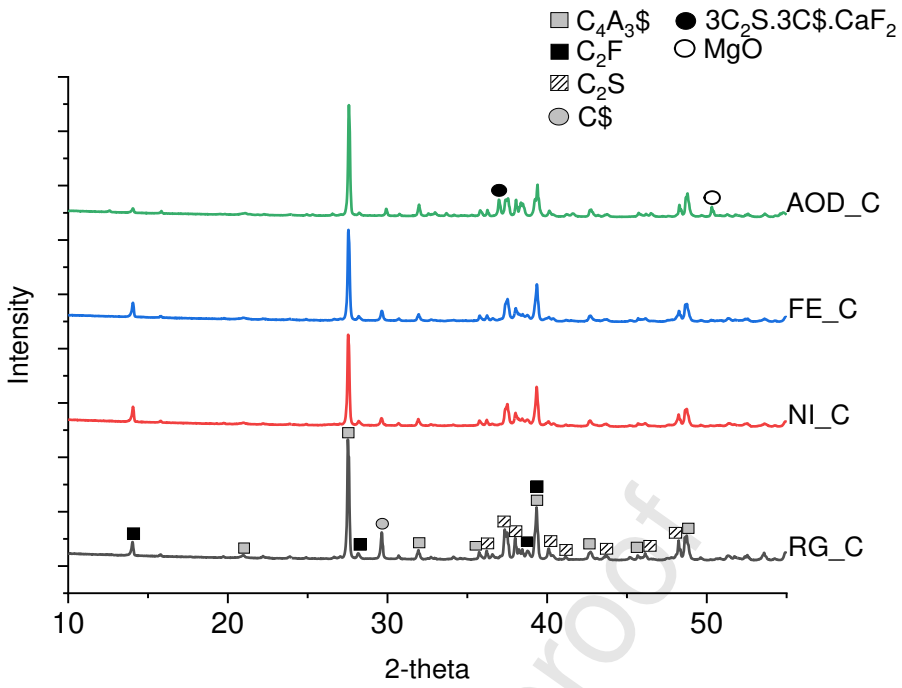

Fig. 2. XRD-patterns (2-theta 10-55°) of synthesized clinkers with main phases $C_4A_3\$$=Ye'elimite, C_2F=Ferrite, (C_2S)=Belite, (C$)=Anhydrite, $3C_2S{\cdot}3C\${\cdot}CaF_2$=Fluorellestadite, and MgO=Periclase measured with Co K_α X-ray source.

Table 6. XRD-WPPF (Whole Powder Pattern Fit) results of produced clinkers, the values are given in %. The quality of analysis is given as weighted profile R-factor (R_{wp}) and the goodness of fit S.

Phase name	**Formula**	**DB card number (PDXL 2)**	**RG_C [%]**	**AOD_C [%]**	**Fay_C [%]**	**Fe_C [%]**
Ye'elimite, cubic (Cuesta et al., 2013)	$Ca_4Al_6(SO_4)O_{12}$	04-019-5778	19.7	26.2	23.8	27.2
Ye'elimite, orthorhombic (Cuesta et al., 2014)	$Ca_4Al_6(SO_4)O_{12}$	01-083-9042	19.7	14	16.6	12.5
Ye'elimite total	$Ca_4Al_6(SO_4)O_{12}$	-	**39.4**	**40.2**	**40.4**	**39.7**
Belite, β (Mumme et al., 1995)	$Ca_2(SiO_4)$	04-007-2687	32.6	19.7	26.4	32.9
Belite, α' (Mumme et al., 1996)	$Ca_2(SiO_4)$	04-017-1330	1.8	3.2	7.5	1.2
Belite total	$Ca_2(SiO_4)$	-	**34.4**	**22.9**	**33.9**	**34.1**

Ferrite (Redhammer et al., 2004)	$Ca_2(Fe_2)O_5$	04-014-6625	18.8	12.3	18.9	19.9
Anhydrite (Morikawa et al., 1975)	$Ca(SO_4)$	04-007-6682	6.7	1.1	5.3	3.9
Mayenite (Palacios et al., 2008)	$Ca_{12}Al_{14}O_{33}$	04-015-5592	0.2	2.9	0	1.6
Fluorellestadite (Pajares et al., 2002)	$Ca_5(SiO_4)_{1.5}(SO_4)_{1.5}F$	04-016-5550	0	14	0	0
Periclase (Sasaki et al., 1979)	MgO	01-071-1176	0.2	3.7	1	0.7
Silicon Dioxide (Ohsumi et al., 1982)	SiO_2	04-008-8250	0.3	0.4	0.5	0.2
Iron (III) oxide (Bykova et al., 2016)	Fe_2O_3	01-085-3771	0	2.3	0	0
		Total	100	100	100	100
		R_{WP}[%]	5.3	4.4	5	5
		S value	2.7	3.6	3.9	3.9

The weighted pattern R-factors (R_{wp}) are in the range 5.0-5.3%, and the goodness of fit indicator, S-value, was between 2.7-3-9. The Rietveld analysis was validated by comparing the back calculation of oxide content from Rietveld measurements with that from XRF analysis of the clinkers and with initial composition, which is the sum of target composition of the clinkers and impurities (MgO and CaF_2) based on the XRF data of the raw materials.

The phase compositions of RG_C, Fay_C, and Fe_C clinkers were close to the target composition (see Table 3); the main phases identified by XRD were ye'elimite ($C_4A_3\$$), belite (C_2S), and Ferrite (C_2F). Both cubic and orthorhombic polymorphs of ye'elimite are present in all clinkers while belite is mostly present as β-C_2S (i.e. larnite). For the analysis, the reference for ferrite phase was selected to be $Ca_2(Fe_2)O_5$ with space group Pnma, because according to Redhammer et al. (2004), pure $Ca_2Fe_{2-x}Al_xO_5$ has space group Pnma up to x=0.56 and I2mb when x>0.56. The minor phases present in clinkers were anhydrite (C$), mayenite ($C_{12}A_7$), periclase (MgO), and unreacted SiO_2.

On the other hand, in AOD_C, part of the belite and ferrite was replaced with unwanted fluorine containing fluorellestadite ($Ca_{10}(SiO_4)_3(SO_4)_3F_2$), with apatite structure; see Table 6. Due to the lower ferrite formation, iron was detected, through XRD it was analysed to be unreacted iron oxide, but later in this study at least some metallic iron particles originating from AOD slag were detected with FESEM-EDS from hydrated

AOD_C clinker. The formation of fluorellestadite can be attributed to the fluorine content of AOD slag. In the study of Adolfsson et al., 2007a fluorellestadite was not detected even though the slag used may have contained fluorine as fluorspar is normally added to AOD converter during the AOD process. When fluorine is present in raw mix, care must be taken for mix design and clinkering conditions in order to avoid melting and fluorellestadite formation. Fluorellestadite should be avoided in the final product because it ties SO_3, SiO_2, and CaO with F and is not cementitious (Blanco-Varela et al., 1995; Hewlett, 2003). According to the literature concerning PC and modified PC, fluorellestadite should decompose at 1240-1250 °C (Blanco-Varela et al., 1995; Hewlett, 2003); however, it seems that in our sample, the fluorellestadite stays stable in AOD_C. AOD_C also had significant amounts (4 wt%) of periclase (MgO) which is an unwanted component but cannot be avoided when using side-stream based raw materials.

The Rietveld analysis presented in Table 6 is validated in Table 7 by comparing the back calculation of oxide content from Rietveld measurements with that from XRF analysis (Table 8) of the clinkers and with initial composition, which is the sum of target composition of the clinkers, including MgO and CaF_2, based on the XRF data of the raw materials (Table 2). For back calculation, the phases considered were: $C_4A_3\$$, C_2S, C_2F, $C\$$, $C_{12}A_7$, $Ca_{10}(SiO_4)_3(SO_4)_3F_2$, MgO, SiO_2, and Fe_2O_3. XRF analysis of the clinkers validates the Rietveld analysis (WPPF) results with desired accuracy. Even for typical phase assemblages the reproducibility of XRD analysis for cement phase is challenging and general uncertainties are in the range 4.1–6.5% (León-Reina et al., 2009).

Possible errors in the analyses are caused by non-detected minor phases, overlapping peaks, atomic impurities, several different polymorphs of the phases and possible analysis errors (León-Reina et al., 2009). From XRF analysis, iron content in Rietveld back calculation is over estimated. The content of Al_2O_3 and Fe_2O_3 differs in back calculation because stoichiometric C_2F was used instead of C_4AF for calculations, and the ferrite phase present contains Al_2O_3. Actual A/F ratios in ferrite are determined with FESEM-EDS later in this study. In back calculation of Fe_C there is less SO_3 when compared to XRF measurements and initial chemical composition. From FESEM-EDS analysis, it was detected that in Fe_C there were barium- and

sulphate-rich grains, probably baryte, which were not detected in XRD data; this must be validated in future studies.

Table 7. Validation of Rietveld analysis (WPPF) by back calculation from Table 6 and XRF of the clinkers to compare the quality of Rietveld, the values are given in %.

Analysis	Sample	CaO	Al_2O_3	SiO_2	Fe_2O_3	SO_3	MgO	CaF_2
	RG_C	48.6	20.3	12.2	10	9		
Initial oxide	AOD_C	48.6	20.3	12.2	10	9	3.8	1.4
composition	Fay_C	48.6	20.3	12.2	10	9	1.1	
	Fe_C	48.6	20.3	12.2	10	9	0.8	
Back	RG_C	47.5	19.8	12.3	11	9.1	0.2	
calculated	AOD_C	43.7	21.6	10.9	9.5	9.3	3.7	1.1
oxide content	Fay_C	46.9	20.2	12.3	11.1	8.4	1	0
from Rietveld	Fe_C	47.4	20.7	12.1	11.7	7.5	0.7	0

Table 8. XRF analysis of prepared clinkers, the values are given in %.

Oxides	RG_C	AOD_C	Fay_C	Fe_C
CaO	47.97	45.82	47.33	46.67
Al_2O_3	19.56	18.86	19.44	19.18
SiO_2	12.22	11.95	12.56	12.60
Fe_2O_3	10.46	9.79	10.25	10.57
SO_3	8.39	8.31	8.16	8.25
MgO	0.26	3.59	1.28	0.98
BaO	0.00	0.00	0.01	0.09

Cl	0.06	0.12	0.13	0.11
Cr_2O_3	0.02	0.23	0.09	0.09
CuO	0.00	0.02	0.06	0.10
K_2O	0.00	0.06	0.10	0.13
MnO	0.00	0.12	0.02	0.19
Na_2O	0.00	0.09	0.17	0.80
NiO	0.01	0.05	0.12	0.07
P_2O_5	0.01	0.00	0.02	0.07
SrO	0.05	0.05	0.05	0.08
TiO_2	0.01	0.17	0.01	0.10
ZnO	0.03	0.04	0.03	0.19
ZrO_2	0.00	0.01	0.01	0.02
Total	99.06	99.27	99.83	100.29

To further confirm results presented in Table 9, the chemical composition of clinkers is calculated through FESEM-EDS to validate the Rietveld and XRF analysis presented in table 6, 7 and 8. The calculation is done by converting detected and analysed weight percent of main phases (($C_4A3\$$, C_2S, C_2F, $Ca_{10}(SiO_4)_3(SO_4)_3F_2$ and MgO) from FESEM-EDS point analysis to oxides and then, the oxide contents are multiplied with the phase contents obtained from Rietveld analysis presented in Table 6. The advantage using FESEM-EDS point when compared to XRD is that the real chemical composition of single phases is used, which also takes foreign ions associated to phases in account. The disadvantage is that undetected/non-analysed minor phases are excluded from analysis.

Table 9. The total chemical composition of clinkers based on average chemical composition of main phases (ye'elimite, larnite, ferrite and fluorellestadite) detected and analysed with FESEM-EDS point analysis and the phase composition determined with Rietveld analysis (Table 6.). The values are given in %.

Oxides	RGC_C	Fay_C	Fe_C	AOD_C
CaO	47.58	44.18	44.65	42.86
Al_2O_3	21.09	21.29	21.98	20.22
SiO_2	13.1	11.54	12.9	11.06
Fe_2O_3	11.05	9.83	9.63	6.66
SO_3	6.15	7	5.75	8.6
MgO	0.01	1.62	1.24	3.45
Na_2O		0.25	0.25	0.05
K_2O		0.29		0.22
MnO		0.09	0.21	0.09
NiO		0.06	0.02	
P_2O_5			0.23	
TiO_2			0.21	0.1
Co_3O_4		0.02		
Cr_2O_3				0.13
F				2.05*
ZnO			0.36	
Total	98.98	96.18	97.15	95.49

*CaF_2=4.2

SO_3 content in table 9 is low in RG_C, Fay_C and Fe_C because anhydrite phase could not be analysed with FESEM-EDS due to insufficient number of EDS-points. In AOD_C, SO_3 is found as fluorellestadite rather than anhydrite allowing the calculated SO_3 content to be closer to target. Iron content in XRF analysis of clinkers is the targeted 10%. The iron content of AOD_C in Table 9 is low because it is not all found as $C_2(A_xF_{1-x})$.

3.3 Characterization with FESEM-EDS

The main phases of RG_C clinker (ye'elimite, belite, and ferrite) detected from a FESEM-BSE image (see Fig. 3) are existing mainly as mono-mineral clusters composed of at least ten of individual mineral grains. The grinding and re-firing could have led to a more homogenous microstructure. The microstructure of Fay_C (not shown) was very similar to RG_C; the only difference was the presence of periclase as a minor phase. FESEM-BSE images of AOD_C and Fe_C are presented in Figs 4 and 5, respectively. The similar main phases, as in RG_C, could be detected from these clinkers.

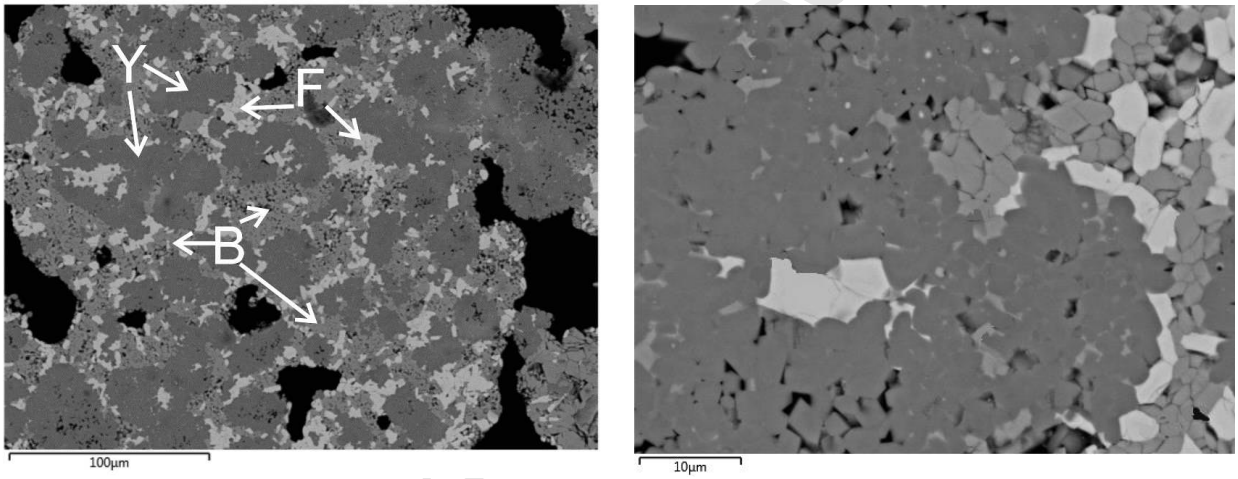

Phase	O	Mg	Al	Si	S	Ca	Fe	Total
B:Belite	35.6		0.3	16.9	0.3	48.9	0.6	101.9
F:Ferrite	30.2	0.3	5.1	0.8	0.3	33.6	34.4	104.2
Y:Ye'elimite	39.9		25.6	0.4	5.8	27.6	2.7	102.0

Fig. 3. Left; overall FESEM-BSE image (x1000) of reference clinker (RG_C). F: ferrite, Y: Ye'elimite, B: Belite, Right; magnification of RG_C (x5000). The average chemical composition (wt%) of phases obtained from FESEM-EDS analysis of 10 selected points from RG_C clinker.

Fluorine containing fluorellestadite ($Ca_{10}(SiO_4)_3(SO_4)_3F_2$) in AOD slag clinker can be identified in Fig 4A by the elemental mapping. Fluorellestadite has lower Si content than belite, higher S content than ye'elimite, and

does not contain any Al. From Fig. 4B, it can be seen that fluorellestadite (dark grey) is located next to ye'elimite (black), and there is also some fluorellestadite inclusion in ye'elimite grains. The ferrite phase is observed as lightest colour in Figs 4A and 4B, and it appears to have filled the empty spaces after formation of larnite/belite, ye'elimite, and fluorellestadite grains.

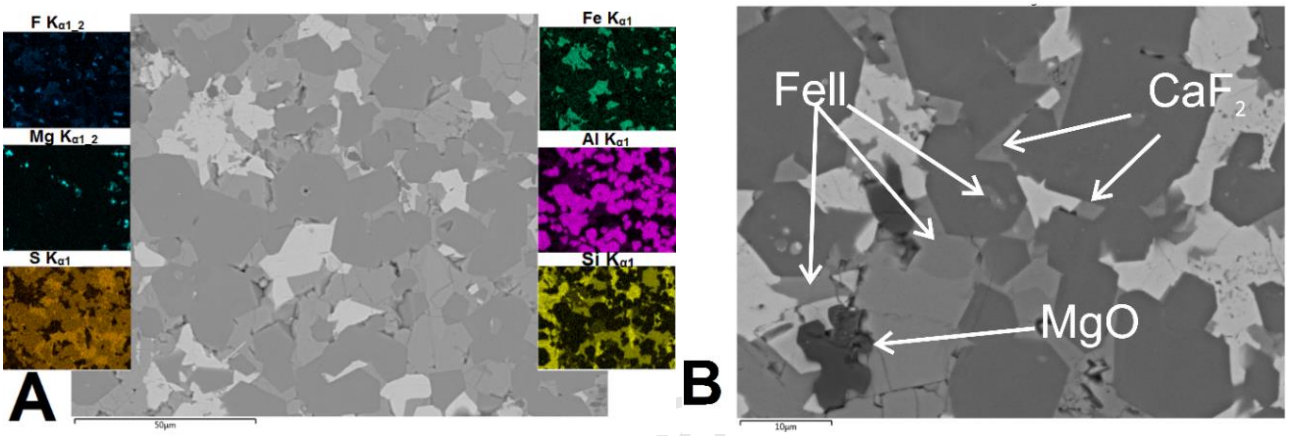

Fig. 4. FESEM-BSE image of AOD_C; (A) with elemental mapping for selected elements (F, Mg, S, Fe, Al, Si), (B) FESEM-BSE image of AOD_C. Fell: fluorellestadite, MgO: Periclase, CaF_2: Fluorite.

The identified phases in Fe_C were ye'elimite, belite (larnite), ferrite, and periclase (Fig. 5A). Barium and sulphate containing white grains were detected with EDS (Fig 5B). Because of the small size of the grains, the EDS analysis was mixed with other surrounding minerals. Although the grains could not be identified accurately, this is probably barium sulphate (baryte).

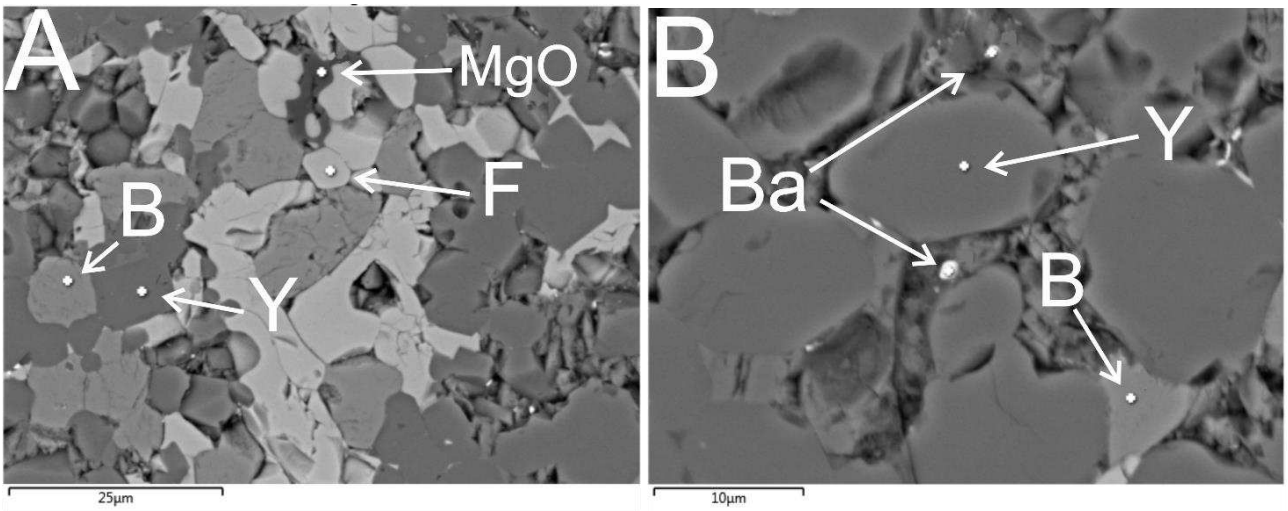

Fig. 5. FESEM-BSE of FE_C; (A) identified phases F: ferrite, Y: Ye'elimite, B: Belite (Larnite), MgO: Periclase, (B) Ba: barium and sulphate containing white grains, Y: Ye'elimite, B: Belite (Larnite).

In the clinkers based on side-streams, impurities were detected in both major and minor phases with EDS point analysis. The impurities present in main phases are presented in Table 10. Due to the high iron content of the original chemical composition of all of the synthesized clinkers, ye'elimite and larnite contained iron as an impurity. According to FESEM-EDS analysis in larnite and ye'elimite, Fe_2O_3 content is between 0.6-1.1 wt% and 2.7-3.6 wt%, respectively. Ye'elimite contained Mg, K, and Na; belite/larnite contained Mg and Na; Ferrite contained Na, Mg, Na, and K, and metals Ti, Cr, and Mn; periclase contained Fe, Ni, Zn and Co.

Table 10. Impurities detected with FESEM-EDS in the clinkers produced from side-streams.

	AOD_C	**Fay_C**	**Fe_C**
Ye'elimite	Mg, K, Fe	Mg, K, Fe	Na, Fe
Larnite	Al, Mg, Fe	Al, Mg, Fe	Al, P, Na, Mg, Fe
Ferrite	Mg, K, Ti, Mn, Cr	Na, Mg, K	Mg, Na, Ti, Mn
Periclase	Fe, Ni	Fe, Ni and Co	Zn and Ni

Fluorellestadite	Mg, Cr, Fe		

The impurities from industrial residues can stabilize different polymorphs of belite (for example α-C_2S, α'_H-C_2S or β-C_2S). In this study, most of the C_2S in the produced clinkers was β-C_2S (i.e. larnite) and only small amounts of α'_H-C_2S were detected with XRD. This means that foreign ions present in the systems studied here are stabilizing larnite which is well in accordance with current literature. The usage of foreign ions to chemically stabilize belite, especially α', α, and β polymorphs, have been widely studied (Benarchid et al., 2004; Chen, 2009; Cuberos et al., 2010; Morsli et al., 2007). According to the review paper prepared by Aranda and De la Torre (2013), oxide components such as SO_3, B_2O_3, Cr_2O_3, Na_2O, MgO, P_2O_5, K_2O, BaO, and MnO_2 can be used to stabilize or to cause distortion to different forms of belite. The stabilization of belite is based on defects in the crystal structure brought about by silicate anion replacements with phosphates and other anions and/or calcium cation substitutions (Fukuda et al., 1995; Morsli et al., 2007).

In the produced clinkers, the ferrite phase contained several different impurities. The average chemical composition of ferrite was analysed by using FESEM-EDS analysis, converted to oxides, and is presented in Table 11. From Table 11, the simplified empirical formula estimated for the ferrite phase is $C_2(A_xF_{1-x})$ with $0.2 \leq x \leq 0.3$ (X_{RG_C} = 0.24, X_{AOD_C}= 0.2, X_{Fay_C}=0.28 and X_{Fe_C}=0.3). The content of foreign ions in ferrite might also promote stability/unreactivity during hydration. According to Table 11, the amount of MgO content in ferrite varied between 0.1-1.7 wt%.

Table 11. The average oxide composition of ferrite in wt% obtained from FESEM-EDS analysis of 10 selected points/clinker.

Oxides	**RG_C**	**Stdev**	**AOD_C**	**Stdev**	**Fay_C**	**Stdev**	**Fe_C**	**Stdev**
CaO	46.8	1.2	43.2	1.1	44.0	2.2	44.3	0.9
Fe_2O_3	50.1	1.2	40.5	2.3	42.9	3.9	40.7	1.0
Al_2O_3	9.2	0.8	5.6	1.1	11.1	1.9	9.3	2.3

MgO	0.1	0.2	1.1	0.9	0.8	0.5	0.9	0.3
SiO_2	1.3	0.6	5.1	0.7	2.1	1.6	5.0	1.7
SO_3	0.1	0.2	2.3	1.4	0.9	1.5	0.1	0.3
TiO_2	-	-	0.9	0.2	-	-	0.9	0.7
MnO	-	-	0.7	0.1	-	-	1.1	0.5
Na_2O	-	-	-	-	0.1	0.2	0.1	0.1
K_2O	-	-	0.3	0.3	0.1	0.1	-	-
Cr_2O_3	-	-	0.2	0.2	-	-	-	-

According to Jupe et al. (2001), doping with Mg might lead to less hydration of ferrite. They concluded that doping might lead to a stabilized, ordered structure with fewer defects. Defects work as sites where hydration can be initiated. In AOD_C and Fe_C, ferrite contained 0.9 wt% of TiO_2. Duvallet et al. (2012) detected that even a low TiO_2 (~0.5%) addition in ferrite slows the setting time slightly when compared to pure ferrite without TiO_2. The low Al_2O_3 content in ferrite might also lead to slow hydration because the main hydration product of ferrite is the aluminium containing mineral ettringite (Meller et al., 2004). In addition, the effect of iron, fluorine, and sulphur contents on phase formation, firing time, and clinkering temperature should be investigated. Further studies on optimised compositions and processing parameters for AOD slag-based clinker are needed and the fluorellestadite formation needs to be minimised/avoided. A promising alternative to utilize AOD slag is to take advantage of the fluorine content to manufacture alite-ye'elimite-ferrite clinker. Hanein et al. (2019) demonstrated that the presence of fluorine, sulphate and iron enhances the mineralization in the C_3S-$C_4A_3\$$-C_4AF system, promoting alite formation at 1250 °C. Duvallet et al. (2014b) successfully produced C_3S-C_2S-$C_4A_3\$$-C_4AF using red mud as raw material and CaF_2 and $CaSO_4$ as fluxes and mineralizers. In current study alite was not formed because there is not enough CaO to form alite and also the fluorine content is not adjusted to be optimal for alite formation.

3.4 Mechanical testing

The reported compressive strength results in Fig. 6 are average values of six tests. After 1 day of curing, Fay_C, FE_C and RG_C mortars reached approximately 20-30 MPa strength, then the strength kept developing to reach >30MPa at 28 days of curing. The lower compressive strength in AOD_C can be attributed to the presence of fluorellestadite which is non-hydraulic. The results of CSAB clinkers are compared to commercial fast setting PC clinker (7 and 28 days of curing) and show that compressive strength of the produced CSAB clinkers is comparable with commercial PC clinker.

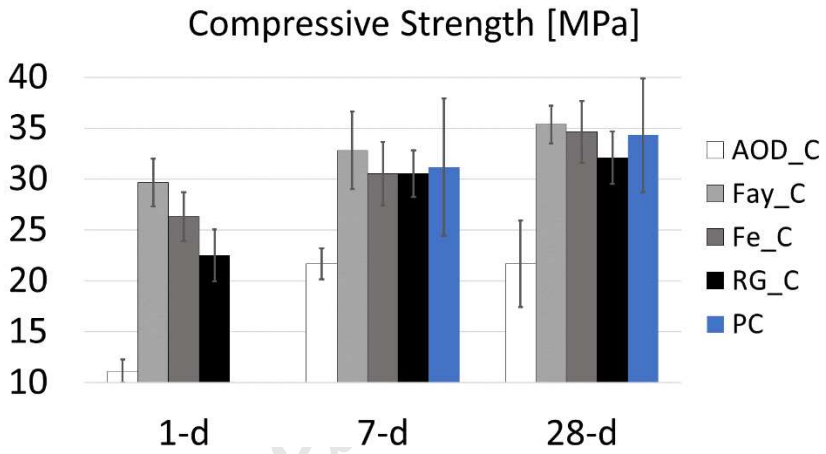

Fig. 6. Compressive strength test results of AOD_C, Fay_C, Fe_C, RG_C and PC (CEM II/A-LL 52.5 N).

The strength development of prepared CSAB clinkers is associated to hydration reaction of ye'elimite together with anhydrite and gypsum to ettringite ($Ca_6Al_2(SO_4)_3(OH)_{12}\cdot 26H_2O$). In Figure 7 the formation of ettringite was confirmed with FESEM-EDS from hydrated RGC_C cement sample after 7 days of curing. The cured samples were prepared by mixing 15% of gypsum with RG_C clinker, water addition with water to cement ratio 0.5 and cured in humidity chamber. After curing the hydration was stopped by immersing crushed (d<4 mm) sample to acetone and the polished section was prepared and analysed with FESEM-EDS with methods mentioned in section 2.2.1. Ettringite appears to be the main phase in cement matrix after 7 days of hydration, but also unreacted cement phases (Belite and Ferrite) could be identified from EDS-

analysis. In EDS-analysis the total sum of ettringite phase is ~90 wt% because hydrogen H cannot be detected with FESEM-EDS.

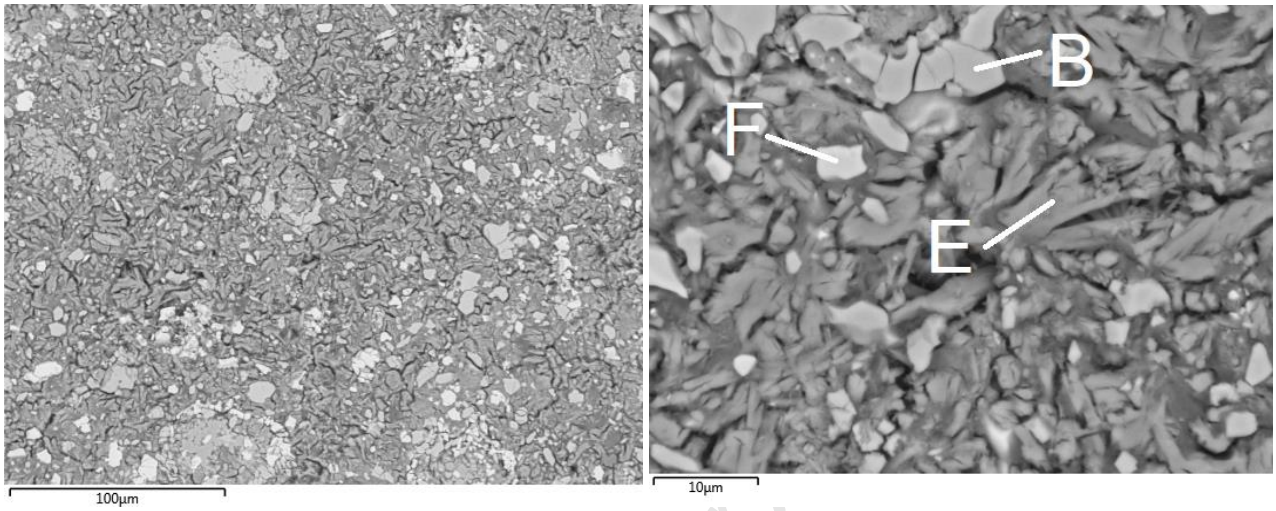

Phase	O	Mg	Al	Si	S	Ca	Fe	Total
B: Belite	36.57		0.2	15.92	0.26	47.07		100.01
F: Ferrite	32.41	0.36	8.32	0.34		31.99	26.09	99.52
E: Ettringite	47.25		12.15	0.91	8.17	20.07		88.54

Figure 7. Left; overall FESEM-BSE-picture (x1000) of RG_C cement sample after 7 days curing. Right; magnification (x5000) with EDS-point analysis of a single point shown in picture, where E: Ettringite, F: ferrite and B: Belite. The values are given in wt%.

Ettringite provides the early strength to hydrated CSAB cement but unreacted ferrite and belite may potentially further increase the mechanical strength upon their hydration. There was a slight increase in mechanical strength between 7 and 28 days with indicates some progress in hydration of these phases. The hydrationand mechanical properties can be further improved by optimization of gypsum and water content and using retarders i.e. tartaric acid and citric acid etc.

According to FESEM studies, the hydration behaviour of Fe_C and Fay_C were very similar to RG_C. High amount of unreacted cement components explains the lower mechanical strength of AOD_C. The

elemental mapping of AOD_C is shown in Fig. 8. In AOD_C there was much more unreacted cement minerals, especially belite and ferrite. The phases presented in Fig. 8, descending from darkest to lightest are ettringite matrix (S, Al, and Ca), larnite grains (Ca and Si), ferrite grains (Fe, Si and Ca), and white particle in the bottom right corner was detected to be metallic iron originating from AOD slag. The presence of unreacted fluorellestadite in AOD_C after 7 days of curing was confirmed with XRD tests.

Figure 8. FESEM-BSE-picture (x3000) of AOD_C cement sample after 7 days curing, where dark grey matrix is ettringite and light grey particles are unreacted clinker phases. White particle in Southeast corner is a metallic particle originating from AOD slag.

3.5 Estimation of raw material amounts to replace Portland cement

The availability of alternative raw materials in certain parts of the world is enough to fulfil a significant amount of virgin, raw cement material demand. These materials are a source of already de-carbonised CaO that can allow for a notable reduction in the carbon footprint of cement manufacture while also promoting a circular economy. It is revealed that more than 10%, perhaps up to 16%, of produced cement in Finland can be replaced through using these alternative raw materials, as estimated in in Table 12. Data for other

countries is not directly available to the authors; however, similar positive impacts may be achieved in countries with a prospering metallurgical industry. Nevertheless, a localized solution for the use of these side-streams and for potentially reducing the cost and carbon footprint of the cement industry is presented. Using single industrial raw material to manufacture clinker is impractical in real applications, because a lot of RGC's or natural materials such as bauxite and calcite are required. It would be much more practical to manufacture clinker from a mix of a few industrial raw materials suggested in this study or alternative materials, which will be studied in the future. Examples of alternative industrial materials to replace RGC's in CSAB clinkers include: phosphogypsum ($CaSO_4$), ladle slag (Al_2O_3, CaO, SiO_2), red mud (Al_2O_3, Fe_2O_3, CaO, SiO_2), metakaolin (Al_2O_3, SiO_2) and fly ash (SiO_2, CaO).

Table 12.Estimated amount of replacement of cement raw materials in Finland with industrial side-streams used for this study.

Material	**Production in Finland [Mt/a]**	**[d] Raw material replacement in CSAB [%]**	**Amount of CSAB cement [Mt/a]**	**[e] Possible PC raw material replacement (Z[Mt/a] /PC produced [Mt/a]) [%]**
Equation	**X**	**Y**	**Z=X*(Y/100%)**	**(Z/1.02Mt/a)*100%**
[a] AOD slag	0.15	43.3	0.065	6.4
[b] Fayalitic slag	0.15	17	0.026	2.5
[c] Jarosite	0.16-0.28	25.3	0.04-0.07	4.0-7.0
Total	0.56-0.68		[d] 0.13-0.16	12.9-15.9

a) Outokumpu stainless steel, 550000t stainless steel produced in Finland, 0.27t AOD slag/1t stainless steel (Perez, 2017.; Zhao et al., 2013); b) Boliden Harjavalta, 32000t nickel matte produced in Finland, 4.5t fayalitic slag/1t Nickel matte (Perez, 2017.; Warner et al., 2007); c) Boliden Kokkola, 315000t zinc produced, 0.5-0.9t Jarosite/1t Zinc (Glinin et al., 2013; de Souza et al., 2007; Perez, 2017); d) according to clinker recipes used in this study; e) Finnsementti cement produced in Finland 1.02 Mt/a (Perez, 2017).

4. Conclusions

The title study reveals how the impurities in metallurgical industry residue materials affect the properties of CSAB cement clinker. CSAB cement prepared from reagent grade chemicals were compared with those prepared separately from certain industrial side-streams. Metallurgical industry residues can be used as alternative raw materials for the manufacture of CSAB cement which may be used in various applications depending on local regulations and standards; however, minor elements in the material will need to be considered.

The use of Fe slag from zinc production and fayalitic slag together with reagent grade chemicals led to the targeted clinker phase assemblage: ye'elimite-belite-ferrite. With blended gypsum, ettringite formation is observed upon hydration and the produced clinkers achieved >30 MPa compressive strength after 7 days of curing. Impurities originating from the raw materials were detected in minor amounts in all major phases of industrial residue-based CSAB clinkers, and those clinkers contain some minor phases such as periclase.

The utilization of stainless-steel refining (AOD) slag containing fluorine led to the formation of a significant amount of a non-hydraulic phase, fluorellestadite; the clinker phase assemblage was: ye'elimite-belite-fluorellestadite-ferrite instead of the targeted composition. The formation of fluorellestadite affected negatively to the mechanical properties and the achieved strength was only 22 MPa after 28 days of curing for the system studied. The unexpected formation of fluorellestadite demonstrates that, when using industrial side-streams, the raw mix design will need more consideration than is conventional and traditional stoichiometric/Bogue-type calculations may not be sufficient for clinkering calculations.

The different material manufacturing/processing methods worldwide can produce side-stream materials with compositions that are varied enough to have a major effect on properties of any produced cement. Care must be taken when adopting procedures and designs created elsewhere; experimental testing may be needed locally to evaluate and confirm the suitability of these materials for use as alternative raw materials in cement manufacture.

Acknowledgements

The CECIRE (1415/31/2015)-project was supported by Business Finland and the following companies: Boliden Harjavalta, Boliden Kokkola, Yara Suomi, Fortum Waste Solutions and Outokumpu Stainless. XRD and FESEM analysis were performed at the Center of Microscopy and Nanotechnology (University of Oulu). The support of Renlund foundation is also appreciated.

References

Adegoloye, G., Beaucour, A.-L., Ortola, S., Noumowé, A., 2015. Concretes made of EAF slag and AOD slag aggregates from stainless steel process: Mechanical properties and durability. Constr. Build. Mater. 76, 313–321. https://doi.org/10.1016/j.conbuildmat.2014.12.007.

Adolfsson, D., Menad, N., Viggh, E., Björkman, B., 2007a. Steelmaking slags as raw material for sulphoaluminate belite cement. Adv. Cem. Res. 19, 147–156. https://doi.org/10.1680/adcr.2007.19.4.147.

Adolfsson, D., Menad, N., Viggh, E., Björkman, B., 2007b. Hydraulic properties of sulphoaluminate belite cement based on steelmaking slags. Adv. Cem. Res. 19, 133–138. https://doi.org/10.1680/adcr.2007.19.3.133.

Álvarez Pinazo, G., 2015. Active Sulpho-belite cements. Hydration mechanisms and mechanical properties. Dissertation (PhD.). The University of Malaga. Available at: https://riuma.uma.es/xmlui/handle/10630/10348 (accessed February 2019).

Álvarez-Pinazo, G., Santacruz, I., León-Reina, L., Aranda, M.A.G., De la Torre, A.G., 2013. Hydration reactions and mechanical strength developments of iron-rich sulfobelite eco-cements. Ind. Eng. Chem. Res. 52, 16606–16614. https://doi.org/10.1021/ie402484e.

Aranda, M.A.G., De la Torre, A.G., 2013. Sulfoaluminate cement, in: F. Pacheco-Torgal, F., Jalali, S., Labrincha, J., John, V.M. (Eds.), Eco-Efficient Concrete. Elsevier, pp. 488–522. https://doi.org/10.1533/9780857098993.4.488.

Benarchid, M.Y., Diouri, A., Boukhari, A., Aride, J., Rogez, J., Castanet, R., 2004. Elaboration and thermal study of iron–phosphorus-substituted dicalcium silicate phase. Cem. Concr. Res. 34, 1873–1879. https://doi.org/10.1016/j.cemconres.2004.01.030.

Bescher, Eric & Kim, J & Ramseyer, Chris & K Vallens, J., 2018. Low carbon footprint pavement: History of use, performance and new opportunities for belitic calcium sulfoaluminate. Proceedings of the 13th International Symposium on Concrete Roads, Berlin, June 2018. Available at: https://www.researchgate.net/publication/326300478_LOW_CARBON_FOOTPRINT_PAVEMENT_HISTORY_OF_USE_PERFORMANCE_AND_NEW_OPPORTUNITIES_FOR_BELITIC_CALCIUM_SULFOALUMINATE (accessed April 2019).

Blanco-Varela, M.T., Palomo, Á., Puertas, F., Vázquez, T., 1995. Influencia de la incorporación conjunta del CaF_2 y del $CaSO_4$ en el proceso de clinkerización. Obtención de nuevos cementos. (Influence of the joint incorporation of CaF_2 and $CaSO_4$ in the clinkerization process. Obtainment of new cements.) Materiales de Construcción, 45(239), 21-39. https://doi.org/10.3989/mc.1995.v45.i239.551.

Bykova, E., Dubrovinsky, L., Dubrovinskaia, N., Bykov, M., McCammon, C., Ovsyannikov, S.V., Liermann, H.-P., Kupenko, I., Chumakov, A.I., Rüffer, R., Hanfland, M., Prakapenka, V., 2016. Structural complexity of simple Fe_2O_3 at high pressures and temperatures. Nat. Commun. 7, 10661. https://doi.org/10.1038/ncomms10661.

Cembureau, 2018. The European Cement Association, Activity report 2018, Brussels. Available at: https://cembureau.eu/media/1818/actvity-report-2018.pdf (accessed august 2019).

Chen, I.A., 2009. Synthesis of portland cement and calcium sulfoaluminate-belite cement for sustainable development and performance. Dissertation (PhD.). The University of Texas. Available at: https://repositories.lib.utexas.edu/handle/2152/7537 (accessed February 2019).

Chen, I.A., Juenger, M.C.G., 2012. Incorporation of coal combustion residuals into calcium sulfoaluminate-belite cement clinkers. Cem. Concr. Compos. 34, 893–902. https://doi.org/10.1016/j.cemconcomp.2012.04.006.

Chrysochoou, M., Dermatas, D., 2006. Evaluation of ettringite and hydrocalumite formation for heavy metal immobilization: literature review and experimental study. J. Hazard Mater. 136, 20-33. https://doi.org/10.1016/j.jhazmat.2005.11.008.

Cuberos, A.J.M., De la Torre, Á.G., Álvarez-Pinazo, G., Martín-Sedeño, M.C., Schollbach, K., Pöllmann, H., Aranda, M.A.G., 2010. Active iron-rich belite sulfoaluminate cements: Clinkering and hydration. Environ. Sci. Technol. 44, 6855–6862. https://doi.org/10.1021/es101785n.

Cuesta, A., De la Torre, A.G., Losilla, E.R., Peterson, V.K., Rejmak, P., Ayuela, A., Frontera, C., Aranda, M.A.G., 2013. Structure, atomistic simulations, and phase transition of stoichiometric ye'elimite. Chem. Mater. 25, 1680–1687. https://doi.org/10.1021/cm400129z.

Cuesta, A., De la Torre, A.G., Losilla E.R., Santacruz, I., Aranda, M.A.G., 2014. Pseudocubic crystal structure and phase transition in doped ye'elimite. Crystal Growth & Design 14(10): 5158–5163. https:doi.org/10.1021/cg501290q.

da Costa, E.B., Rodríguez, E.D., Bernal, S.A., Provis, J.L., Gobbo, L.A., Kirchheim, A.P., 2016. Production and hydration of calcium sulfoaluminate-belite cements derived from aluminium anodising sludge. Constr. Build. Mater. 122, 373–383. https://doi.org/10.1016/j.conbuildmat.2016.06.022.

de Souza, A.D., Pina, P.S., Leão, V.A., 2007. Bioleaching and chemical leaching as an integrated process in the zinc industry. Miner. Eng. 20, 591–599. https://doi.org/10.1016/j.mineng.2006.12.014.

Di Maria, A., Salman, M., Dubois, M., Van Acker, K., 2018. Life cycle assessment to evaluate the environmental performance of new construction material from stainless steel slag. Int. J. Life Cycle Assess. 23, 2091–2109. https://doi.org/10.1007/s11367-018-1440-1.

Durinck, D., Arnout, S., Mertens, G., Boydens, E., Jones, P.T., Elsen, J., Blanpain, B., Wollants, P., 2008. Borate distribution in stabilized stainless-steel slag. J. Am. Ceram. Soc. 91, 548–554. https://doi.org/10.1111/j.1551-2916.2007.02147.x.

Dutrizac, J.E., 1984. The behavior of impurities during jarosite precipitation, in: Bautista, R.G. (Ed.), Hydrometallurgical Process Fundamentals, NATO Conference Series. Springer US, Boston, MA, pp. 125–169. https://doi.org/10.1007/978-1-4899-2274-8_6.

Duvallet, T., 2014a. Influence of ferrite phase in alite-calcium sulfoaluminate cements. Theses and Dissertations-Chemical and Materials Engineering 27. Available at: https://uknowledge.uky.edu/cme_etds/27/ (accessed February 2019).

Duvallet, T., Zhou Y., Robl L., Andrews R., 2014b. Synthesis and characterization of high-iron alite-calcium sulfoaluminate-ferrite cements produced from industrial by-products. Coal Combustion and Gasification Products 5, 29-32, doi: 10.4177/CCGP-D-14-00007.1.

Duvallet, T., Robl, T.L., Glasser, F.P., 2012. The effect of titanium dioxide on the structure and reactivity of ferrite. 8th International Conference: Concrete in the Low Carbon Era, Dundee, UK, 2012.

El-Alfi, E.A., Gado, R.A., 2016. Preparation of calcium sulfoaluminate-belite cement from marble sludge waste. Constr. Build. Mater. 113, 764–772. https://doi.org/10.1016/j.conbuildmat.2016.03.103.

EN 196-1, 2005. Methods of testing cement – Part 1: Determination of strength

Fukuda, K., Maki, I., Ito, S., Toyoda, K., 1995. Kinetics of remelting reaction in Ca_2Sio_4 solid solutions. J. Ceram. Soc. Jpn. 103, 444–448.

Geller, S., Grant, R.W., Gonser, U., 1971. Crystal chemistry and magnetic structures of substituted $Ca_2[Fe](Fe)O_5$. Prog. Solid State Chem. 5, 1–26. https://doi.org/10.1016/0079-6786(71)90015-X.

Gartner, E., Hirao, H., 2015. A review of alternative approaches to the reduction of CO_2 emissions associated with the manufacture of the binder phase in concrete. Cem. Concr. Res., Keynote papers from 14th International Congress on the Chemistry of Cement (ICCC 2015) 78, Part A, 126–142. https://doi.org/10.1016/j.cemconres.2015.04.012.

Glinin, A., Creedy, S., Matusewicz, R., Hughes, S., Reuter, M., 2013. Outotec® ausmelt technology for treating zinc residues. In Proceedings of the European Metal Conference EMC 2013, Lead-Zinc Volume, pp. 485-493. Available at: https://www.researchgate.net/profile/Markus_Reuter3/publication/270048746_Ausmelt_Technology_for_Treating_Zinc_Residues/links/549eacca0cf202801ea821b5/Ausmelt-Technology-for-Treating-Zinc-Residues.pdf (accessed February 2019).

Hanein, T., Duvallet, T.Y., Jewell, R.B., Oberlink, A.E., Robl, T.L., Zhou, Y., Glasser, F.P., Bannerman, M.N., 2019. Alite calcium sulfoaluminate cement: chemistry and thermodynamics. Adv. Cem. Res. 31(3), 94-105.https://doi.org/10.1680/jadcr.18.00118

Hanein, T., Galan, I., Elhoweris, A., Khare, S., Skalamprinos, S., Jen, G., Whittaker, M., Imbabi, M.S., Glasser, F.P., Bannerman, M.N., 2016. Production of belite calcium sulfoaluminate cement using sulfur as a fuel and as a source of clinker sulfur trioxide: pilot kiln trial. Adv. Cem. Res. 28, 643–653. https://doi.org/10.1680/jadcr.16.00018.

Hanein, T., Galvez-Martos, J.-L., Bannerman, M.N., 2018. Carbon footprint of calcium sulfoaluminate clinker production. J. Clean. Prod. 172, 2278–2287. https://doi.org/10.1016/j.jclepro.2017.11.183.

Hewlett, P., 2003. Lea's chemistry of cement and concrete. Lea's Chemistry of Cement and Concrete. 4th ed. edited by Peter C. Hewlett. Oxford : Butterworth-Heinemann, 2001. 4th edition. pp. 225 and 585. https://doi.org/10.1016/B978-0-7506-6256-7.X5007-3.

Huaiwei, Z., Xin, H., 2011. An overview for the utilization of wastes from stainless steel industries. Resour. Conserv. Recycl. 55, 745–754. https://doi.org/10.1016/j.resconrec.2011.03.005.

Iacobescu, R.I., Pontikes, Y., Koumpouri, D., Angelopoulos, G.N., 2013. Synthesis, characterization and properties of calcium ferroaluminate belite cements produced with electric arc furnace steel slag as raw material. Cem. Concr. Compos. 44, 1–8. https://doi.org/10.1016/j.cemconcomp.2013.08.002.

Jupe, A.C., Cockcroft, J.K., Barnes, P., Colston, S.L., Sankar, G., Hall, C., 2001. The site occupancy of Mg in the brownmillerite structure and its effect on hydration properties: an X-ray/neutron diffraction and EXAFS study. J. Appl. Crystallogr. 34, 55–61. https://doi.org/10.1107/S0021889800016095.

Kiventerä, J., Piekkari, K., Isteri, V., Ohenoja, K., Tanskanen, P., Illikainen, M., 2019. Solidification/stabilization of gold mine tailings using calcium sulfoaluminate-belite cement. J. Clean. Prod. 239. https://doi.org/10.1016/j.jclepro.2019.118008.

Kumarathasan, P., McCarthy, G.J., Hassett, D.J., Pflughoeft-Hassett, D.F., 1989. Oxyanion substituted ettringites: synthesis and characterization; and their potential role in immobilization of as, B, Cr, Se and V. MRS Proc. 178. In: https://doi.org/10.1557/PROC-178-83.

León-Reina, L., De la Torre, A.G., Porras-Vázquez, J.M., Cruz, M., Ordonez, L.M., Alcobé, X., Gispert-Guirado, F., Larrañaga-Varga, A., Paul, M., Fuellmann, T., Schmidt, R., Aranda, M. a. G., 2009. Round robin on Rietveld quantitative phase analysis of Portland cements. J. Appl. Crystallogr. 42, 906–916. https://doi.org/10.1107/S0021889809028374

Maragkos, I., Giannopoulou, I.P., Panias, D., 2009. Synthesis of ferronickel slag-based geopolymers. Min. eng. 22 196-203. https://doi.org/10.1016/j.mineng.2008.07.003

Meller, N., Hall, C., Jupe, A.C., Colston, S.L., Jacques, S.D.M., Barnes, P., Phipps, J., 2004. The paste hydration of brownmillerite with and without gypsum: a time resolved synchrotron diffraction study at 30, 70, 100 and 150 °C. J. Mater. Chem. 14, 428–435. https://doi.org/10.1039/B313215C.

Miller, S.A., Horvath, A., Monteiro, P.J.M., 2016. Readily implementable techniques can cut annual CO2 emissions from the production of concrete by over 20%. Environ. Res. Lett. 11. https://doi.org/10.1088/1748-9326/11/7/074029.

Miller, S.A., John, V.M., Pacca, S.A., Horvath, A., 2018. Carbon dioxide reduction potential in the global cement industry by 2050. Cem. Concr. Res. 114, 115–124. https://doi.org/10.1016/j.cemconres.2017.08.026.

Morikawa, H., Minato, I., Tomita, T., Iwai, S., 1975. Anhydrite: a refinement. Acta Crystallogr. B 31, 2164–2165. https://doi.org/10.1107/S0567740875007145.

Morsli, K., Torre, Á.G.D.L., Stöber, S., Cuberos, A.J.M., Zahir, M., Aranda, M.A.G., 2007. Quantitative phase analysis of laboratory-active belite clinkers by synchrotron powder diffraction. J. Am. Ceram. Soc. 90, 3205–3212. https://doi.org/10.1111/j.1551-2916.2007.01870.x.

Mumme, W., Cranswick, L.M.D., Chakoumakos, B., 1996. Rietveld crystal structure refinements from high temperature neutron powder diffraction data for the polymorphs of dicalcium silicate. Neues Jahrb. Mineral. Abh. 170, 171–188.

Mumme, W., Hill, R., Bushnellwye, G., Segnit, E., 1995. Rietveld crystal-structure refinements, crystal-chemistry and calculated powder diffraction data for the polymorphs of dicalcium silicate and related phases. Neues Jahrb. Mineral.-Abh. 169, 35–68.

Odler, I., Zhang, H., 1996. Investigations on high SO3 portland clinkers and cements I. Clinker synthesis and cement preparation. Cem. Concr. Res. 26, 1307–1313. https://doi.org/10.1016/0008-8846(96)00128-7.

Ohsumi, K., Sawada, T., Takeuchi, Y., Sadanaga, R., 1982. Development of laser-heating device for single crystal diffractometry and the structure of high cristobalite. J. Jpn. Assoc. Mineral. Petrol. Econ. Geol. 77, 349–355.

Pajares, I., Torre, Á.G.D. la, Martínez-Ramírez, S., Puertas, F., Blanco-Varela, M.-T., Aranda, M.A.G., 2002. Quantitative analysis of mineralized white portland clinkers: The structure of Fluorellestadite. Powder Diffr. 17, 281–286. https://doi.org/10.1154/1.1505045.

Palacios, L., Cabeza, A., Bruque, S., García-Granda, S., Aranda, M.A.G., 2008. Structure and electrons in mayenite electrides. Inorg. Chem. 47, 2661–2667. https://doi.org/10.1021/ic7021193.

Perez, A.A., 2017. U.S. Geological survey, minerals yearbook 2014, Finland. Available at: https://minerals.usgs.gov/minerals/pubs/country/2014/myb3-2014-fi.pdf (accessed February 2019).

Peysson, S., P_era, J., Chabannet, M., 2005. Immobilization of heavy metals by calcium sulfoaluminate cement. Cement Concr. Res. 35, 2261e2270. https://doi.org/10.1016/j.cemconres.2005.03.015.

Rahman, M.A., Sarker, P.K., Shaikh, F.U.A., Saha, A.K., 2017. Soundness and compressive strength of Portland cement blended with ground granulated ferronickel slag. Constr. Build. Mater. 140, 194–202. https://doi.org/10.1016/j.conbuildmat.2017.02.023.

Redhammer, G.J., Tippelt, G., Roth, G., Amthauer, G., 2004. Structural variations in the brownmillerite series $Ca_2(Fe_{2-x}Al_x)O_5$: Single-crystal X-ray diffraction at 25 °C and high-temperature X-ray powder diffraction (25 °C ≤ T ≤ 1000 °C). Am. Mineral. 89, 405–420. https://doi.org/10.2138/am-2004-2-322.

Rämä, M., Nurmi, S., Jokilaakso, A., Klemettinen, L., Taskinen, P., Salminen, J., 2018. Thermal processing of jarosite leach residue for a safe disposable slag and valuable metals recovery. Metals 8, 744. https://doi.org/10.3390/met8100744.

Scrivener, K.L., John, V.M., Gartner, E.M., 2018. Eco-efficient cements: Potential economically viable solutions for a low-CO_2 cement-based materials industry. Cem. Concr. Res. 114, 2–26. https://doi.org/10.1016/j.cemconres.2018.03.015.

Sasaki, S., Fujino, K., Takéuchi, Y., 1979. X-Ray determination of electron-density distributions in oxides, MgO, MnO, CoO, and NiO, and atomic scattering factors of their constituent atoms. Proc. Jpn. Acad. Ser. B 55, 43–48. https://doi.org/10.2183/pjab.55.43.

Seki A., Aso Y., Okubo M., Sudo F., Ishizaka K., 1986. Development of dusting prevention stabilizer for stainless steel slag. Kawasaki technical report No. 15 October 1986, pages 16-21. Available at: http://www.jfe-steel.co.jp/archives/en/ksc_giho/no.15/e15-016-021.pdf (accessed February 2019).

Shame, E.G., Glasser, F.P., 1987. Stable Ca3SiO5 solid solutions containing fluorine and aluminium made between 1050 and 1250 °C. Br. Ceram. Trans. J. 86(1):13. Br. Ceram. Trans. J. 86, 13–17.

Shen, H., Forssberg, E., Nordström, U., 2004. Physicochemical and mineralogical properties of stainless steel slags oriented to metal recovery. Resour. Conserv. Recycl. 40, 245–271. https://doi.org/10.1016/S0921-3449(03)00072-7.

Smith, D.K., 1962. Crystallographic changes with the substitution of aluminum for iron in dicalcium ferrite. Acta Crystallogr. 15, 1146–1152. https://doi.org/10.1107/S0365110X62003011

Taylor, H.F.W., 1997. Cement chemistry. Thomas Telford. DOI: 10.1680/cc.25929.

United Nations environment programme (UNEP) - Sustainable Buildings & Climate Initiative (SBCI), 2017. Eco-efficient cements: Potential economically viable solutions for a low-CO2 cement-based materials industry. Available at: http://www.greeningtheblue.org/sites/default/files/Buildings%20and%20climate%20change_0.pdf (accessed April 2019).

United States Environmental Protection Agency, 2007. Method 3051A: microwave assisted acid digestion of sediments, sludges, soils, and oils, part of test methods for evaluating solid waste, physical/chemical methods. Available at: https://www.epa.gov/sites/production/files/2015-12/documents/3051a.pdf (accessed February 2019).

Warner, A.E.M., Díaz, C.M., Dalvi, A.D., Mackey, P.J., Tarasov, A.V., Jones, R.T., 2007. JOM world nonferrous smelter survey Part IV: Nickel: Sulfide. JOM 59, 58–72. https://doi.org/10.1007/s11837-007-0056-x.

WBCSD, I., 2009. Cement technology roadmap 2009: carbon emissions reductions up to 2050. World Bus. Counc. Sustain. Dev. Int. Energy Agency. Available at: http://www.wbcsdcement.org/pdf/technology/WBCSD-

IEA_Cement%20Roadmap.pdf.https://www.iea.org/publications/freepublications/publication/Cement.pdf (accessed February 2019).

Zhang, L., Su, M., Wang, Y., 1999. Development of the use of sulfo- and ferroaluminate cements in China. Adv. Cem. Res. 11, 15–21. https://doi.org/10.1680/adcr.1999.11.1.15.

Zhao, H., Qi, Y., Shi, Y., Na, X., Feng, H., 2013. Mechanism and prevention of disintegration of AOD stainless steel slag. J. Iron Steel Res. Int. 20, 26–30. https://doi.org/10.1016/S1006-706X(13)60078-3.

There is no conflict of interest.

All the authors have approved the manuscript and agree with its submission to Special Issue "Circular economy and environment with emphasis on waste management & resource valorization" of the Science of the Total Environment.

The CECIRE (1415/31/2015)-project was supported by Business Finland and the following companies: Boliden Harjavalta, Boliden Kokkola, Yara Suomi, Fortum Waste Solutions and Outokumpu Stainless. XRD and FESEM analysis were performed at the Center of Microscopy and Nanotechnology (University of Oulu).

The permission to publish have a permission from the supporting companies.

Table 1. Details of reagent grade chemicals used for clinker synthesis.

		Purity (wt%)	CAS-number
Aluminium oxide (metals basis), fine powder	Al_2O_3	99	12553
Silicon (IV) Oxide (metals basis), Mesh fused amorphous powder	SiO_2	99	89709
Iron (III) oxide (metals basis)	Fe_2O_3	98	012375
Calcium sulphate, anhydrous powder	$CaSO_4$	99	40144
Calcium oxide, reagent-grade powder	CaO	98	33299

Table 2. Analysis of side-stream raw materials.

XRF oxide composition wt%			
Compounds for CSAB	AOD slag	Fayalitic slag	Fe slag
CaO	53.2	1.8	16.8
SiO_2	28.0	33.5	29.9
FeO	0.6	52.9	35.5
Al_2O_3	1.7	2.3	5.0
SO_3	0.4	0.2	0.8
Other compounds			
MgO	8.72	6.23	3.01
TiO_2	0.34	0.15	0.49
CaF_2	3.2	0.0	0.0
Na_2O	0.0	0.39	2.75
Others (wt. % < 0.8)	1.19	2.3	3.7
ICP analysis results wt%			
Ba	0.02	<0.01	0.53
Mn	0.14	0.02	0.46
Cr	0.08	0.04	0.05
Cu	<0.01	0.06	0.25
Ni	<0.01	<0.4	0.05
Co	<0.01	<0.4	0.02
Zn	<0.01	0.02	0.51

Table 3. Phase composition of target CSAB clinker and corresponding oxide composition.

Target phase composition					
Phase	C_2F	$C_4A_3\$$	C_2S	C$	C
[wt%]	17	41	35	6	1
Corresponding oxide composition					
Oxide	Fe_2O_3	Al_2O_3	SiO_2	SO_3	CaO
[wt%]	10	20	12	9	49

Table 4. Clinker recipes, the values are given in %.

Sample	RG_C	AOD_C	Fay_C	Fe_C
AOD slag		43.3		
Fayalitic slag			17	
Fe slag				25.3
Al_2O_3	20.3	19.5	19.9	19
SiO_2	12.2		6.5	4.6
$CaSO_4$	15.3	15	15.2	15
CaO	42.3	18.4	42	38.2
Fe_2O_3	10	9.7		
SUM + Impurities [%]	100	105.9	100.6	102.1

Table 5. The impurities from raw materials to clinkers, the values are given in %.

XRF	AOD_C	Fay_C	Fe_C
MgO	3.77	1.05	0.78
K_2O	0.13	0.09	0.10
TiO_2	0.13	0.03	0.13
CaF_2	1.37	n.d.	n.d.
Na_2O	n.d.	0.07	0.71
ICP	AOD_C	Fay_C	Fe_C
Ba	<0.01	<0.01	0.13
Mn	0.06	<0.01	0.12
Cr	0.03	<0.01	0.01
Cu	<0.01	<0.01	0.06
Ni	<0.01	0.02	0.01
Co	<0.01	0.01	<0.01

Table 6. XRD-WPPF (Whole Powder Pattern Fit) results of produced clinkers, the values are given in %. The quality of analysis is given as weighted profile R-factor (R_{wp}) and the goodness of fit S.

Phase name	**Formula**	**DB card number (PDXL 2)**	**RG_C [%]**	**AOD_C [%]**	**Fay_C [%]**	**Fe_C [%]**
Ye'elimite, cubic (Cuesta et al., 2013)	$Ca_4Al_6(SO_4)O_{12}$	04-019-5778	19.7	26.2	23.8	27.2
Ye'elimite, orthorhombic (Cuesta et al., 2014)	$Ca_4Al_6(SO_4)O_{12}$	01-083-9042	19.7	14	16.6	12.5
Ye'elimite total	$Ca_4Al_6(SO_4)O_{12}$	-	**39.4**	**40.2**	**40.4**	**39.7**
Belite, β (Mumme et al., 1995)	$Ca_2(SiO_4)$	04-007-2687	32.6	19.7	26.4	32.9
Belite, α' (Mumme et al., 1996)	$Ca_2(SiO_4)$	04-017-1330	1.8	3.2	7.5	1.2
Belite total	$Ca_2(SiO_4)$	-	**34.4**	**22.9**	**33.9**	**34.1**
Ferrite (Redhammer et al., 2004)	$Ca_2(Fe_2)O_5$	04-014-6625	18.8	12.3	18.9	19.9
Anhydrite (Morikawa et al., 1975)	$Ca(SO_4)$	04-007-6682	6.7	1.1	5.3	3.9
Mayenite (Palacios et al., 2008)	$Ca_{12}Al_{14}O_{33}$	04-015-5592	0.2	2.9	0	1.6
Fluorellestadite (Pajares et al., 2002)	$Ca_5(SiO_4)_{1.5}(SO_4)_{1.5}F$	04-016-5550	0	14	0	0
Periclase (Sasaki et al., 1979)	MgO	01-071-1176	0.2	3.7	1	0.7
Silicon Dioxide (Ohsumi et al., 1982)	SiO_2	04-008-8250	0.3	0.4	0.5	0.2
Iron (III) oxide (Bykova et al., 2016)	Fe_2O_3	01-085-3771	0	2.3	0	0
		Total	100	100	100	100
		R_{WP}[%]	5.3	4.4	5	5
		S value	2.7	3.6	3.9	3.9

Table 7. Validation of Rietveld analysis (WPPF) by back calculation from Table 6 and XRF of the clinkers to compare the quality of Rietveld, the values are given in %.

Analysis	Sample	CaO	Al_2O_3	SiO_2	Fe_2O_3	SO_3	MgO	CaF_2
Initial oxide composition	RG_C	48.6	20.3	12.2	10	9		
	AOD_C	48.6	20.3	12.2	10	9	3.8	1.4
	Fay_C	48.6	20.3	12.2	10	9	1.1	
	Fe_C	48.6	20.3	12.2	10	9	0.8	
Back calculated oxide content from Rietveld	RG_C	47.5	19.8	12.3	11	9.1	0.2	
	AOD_C	43.7	21.6	10.9	9.5	9.3	3.7	1.1
	Fay_C	46.9	20.2	12.3	11.1	8.4	1	0
	Fe_C	47.4	20.7	12.1	11.7	7.5	0.7	0

Table 8. XRF analysis of prepared clinkers, the values are given in %.

Oxides	**RG_C**	**AOD_C**	**Fay_C**	**Fe_C**
CaO	47.97	45.82	47.33	46.67
Al_2O_3	19.56	18.86	19.44	19.18
SiO_2	12.22	11.95	12.56	12.60
Fe_2O_3	10.46	9.79	10.25	10.57
SO_3	8.39	8.31	8.16	8.25
MgO	0.26	3.59	1.28	0.98
BaO	0.00	0.00	0.01	0.09
Cl	0.06	0.12	0.13	0.11
Cr_2O_3	0.02	0.23	0.09	0.09
CuO	0.00	0.02	0.06	0.10
K_2O	0.00	0.06	0.10	0.13
MnO	0.00	0.12	0.02	0.19
Na_2O	0.00	0.09	0.17	0.80
NiO	0.01	0.05	0.12	0.07
P_2O_5	0.01	0.00	0.02	0.07
SrO	0.05	0.05	0.05	0.08
TiO_2	0.01	0.17	0.01	0.10
ZnO	0.03	0.04	0.03	0.19
ZrO_2	0.00	0.01	0.01	0.02
Total	99.06	99.27	99.83	100.29

Table 9. The total chemical composition of clinkers based on average chemical composition of main phases (ye'elimite, larnite, ferrite and fluorellestadite) detected and analysed with FESEM-EDS point analysis and the phase composition determined with Rietveld analysis (Table 6.). The values are given in %.

Oxides	**RGC_C**	**Fay_C**	**Fe_C**	**AOD_C**
CaO	47.58	44.18	44.65	42.86
Al_2O_3	21.09	21.29	21.98	20.22
SiO_2	13.1	11.54	12.9	11.06
Fe_2O_3	11.05	9.83	9.63	6.66
SO_3	6.15	7	5.75	8.6
MgO	0.01	1.62	1.24	3.45
Na_2O		0.25	0.25	0.05
K_2O		0.29		0.22
MnO		0.09	0.21	0.09
NiO		0.06	0.02	
P_2O_5			0.23	
TiO_2			0.21	0.1
Co_3O_4		0.02		
Cr_2O_3				0.13
F				2.05*
ZnO			0.36	
Total	98.98	96.18	97.15	95.49

*CaF_2=4.2

Table 10. Impurities detected with FESEM-EDS in the clinkers produced from side-streams.

	AOD_C	**Fay_C**	**Fe_C**
Ye'elimite	Mg, K, Fe	Mg, K, Fe	Na, Fe
Larnite	Al, Mg, Fe	Al, Mg, Fe	Al, P, Na, Mg, Fe
Ferrite	Mg, K, Ti, Mn, Cr	Na, Mg, K	Mg, Na, Ti, Mn
Periclase	Fe, Ni	Fe, Ni and Co	Zn and Ni
Fluorellestadite	Mg, Cr, Fe		

Table 11. The average oxide composition of ferrite in wt% obtained from FESEM-EDS analysis of 10 selected points/clinker.

Oxides	RG_C	Stdev	AOD_C	Stdev	Fay_C	Stdev	Fe_C	Stdev
CaO	46.8	1.2	43.2	1.1	44.0	2.2	44.3	0.9
Fe_2O_3	50.1	1.2	40.5	2.3	42.9	3.9	40.7	1.0
Al_2O_3	9.2	0.8	5.6	1.1	11.1	1.9	9.3	2.3
MgO	0.1	0.2	1.1	0.9	0.8	0.5	0.9	0.3
SiO_2	1.3	0.6	5.1	0.7	2.1	1.6	5.0	1.7
SO_3	0.1	0.2	2.3	1.4	0.9	1.5	0.1	0.3
TiO_2	-	-	0.9	0.2	-	-	0.9	0.7
MnO	-	-	0.7	0.1	-	-	1.1	0.5
Na_2O	-	-	-	-	0.1	0.2	0.1	0.1
K_2O	-	-	0.3	0.3	0.1	0.1	-	-
Cr_2O_3	-	-	0.2	0.2	-	-	-	-

Table 12.Estimated amount of replacement of cement raw materials in Finland with industrial side-streams used for this study.

Material	Production in Finland [Mt/a]	[d] Raw material replacement in CSAB [%]	Amount of CSAB cement [Mt/a]	[e] Possible PC raw material replacement (Z[Mt/a] /PC produced [Mt/a]) [%]
Equation	**X**	**Y**	**Z=X*(Y/100%)**	**(Z/1.02Mt/a)*100%**
[a] AOD slag	0.15	43.3	0.065	6.4
[b] Fayalitic slag	0.15	17	0.026	2.5
[c] Jarosite	0.16-0.28	25.3	0.04-0.07	4.0-7.0
Total	0.56-0.68		[d] 0.13-0.16	12.9-15.9

a) Outokumpu stainless steel, 550000t stainless steel produced in Finland, 0.27t AOD slag/1t stainless steel (Perez, 2017.; Zhao et al., 2013); b) Boliden Harjavalta, 32000t nickel matte produced in Finland, 4.5t fayalitic slag/1t Nickel matte (Perez, 2017.; Warner et al., 2007); c) Boliden Kokkola, 315000t zinc produced, 0.5-0.9t Jarosite/1t Zinc (Glinin et al., 2013; de Souza et al., 2007; Perez, 2017); d) according to clinker recipes used in this study; e) Finnsementti cement produced in Finland 1.02 Mt/a (Perez, 2017).

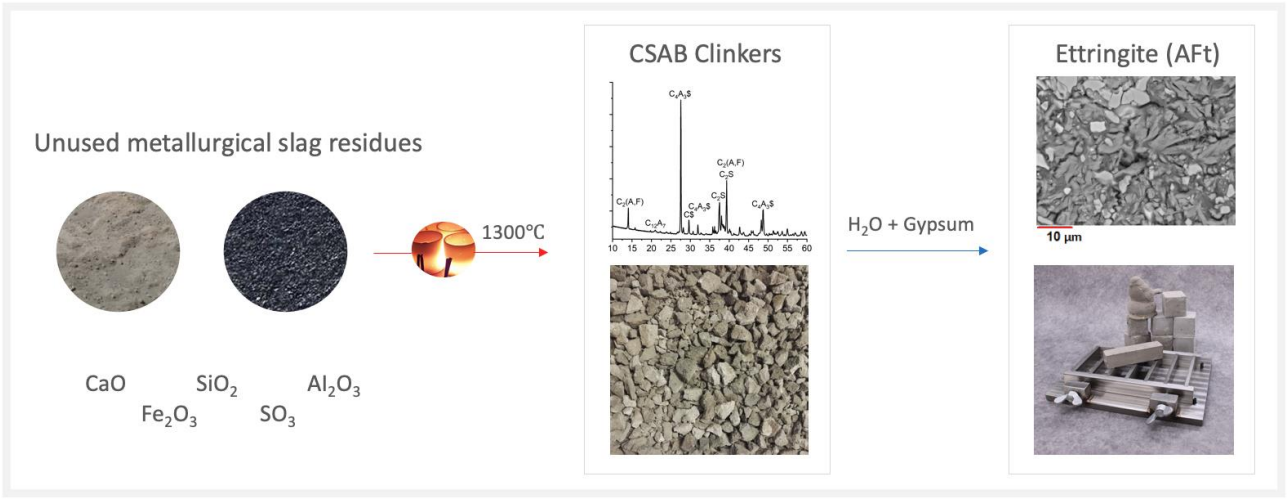

Graphical abstract

Highlights

- CSAB clinkers were produced using metallurgical residues
- Fe and fayalitic slag are used to make CSAB with ye'elimite, belite, and ferrite
- The fluorine content in AOD slag enabled the formation of fluorellestadite
- Compressive strength of the produced CSAB mortars is comparable to commercial PC